NEURODEVELOPMENT

A human DCC variant causing mirror movement disorder reveals that the WAVE regulatory complex mediates axon guidance by netrin-1–DCC

Karina Chaudhari[1]†‡, Kaiyue Zhang[2,3]†, Patricia T. Yam[2], Yixin Zang[1], Daniel A. Kramer[4], Sarah Gagnon[1], Sabrina Schlienger[2,5], Sara Calabretta[2], Jean-Francois Michaud[2], Meagan Collins[6], Junmei Wang[7], Myriam Srour[8,9,6], Baoyu Chen[4], Frédéric Charron[2,3,5,10]*, Greg J. Bashaw[1]*

The axon guidance cue netrin-1 signals through its receptor DCC (deleted in colorectal cancer) to attract commissural axons to the midline. Variants in DCC are frequently associated with congenital mirror movements (CMMs). A CMM-associated variant in the cytoplasmic tail of DCC is located in a conserved motif predicted to bind to a regulator of actin dynamics called the WAVE (Wiskott-Aldrich syndrome protein–family verprolin homologous protein) regulatory complex (WRC). Here, we explored how this variant affects DCC function and may contribute to CMM. We found that a conserved WRC-interacting receptor sequence (WIRS) motif in the cytoplasmic tail of DCC mediated the interaction between DCC and the WRC. This interaction was required for netrin-1–mediated axon guidance in cultured rodent commissural neurons. Furthermore, the WIRS motif of Fra, the *Drosophila* DCC ortholog, was required for attractive signaling in vivo at the *Drosophila* midline. The CMM-associated R1343H variant of DCC, which altered the WIRS motif, prevented the DCC-WRC interaction and impaired axon guidance in cultured commissural neurons and in *Drosophila*. The findings reveal the WRC as a pivotal component of netrin-1–DCC signaling and uncover a molecular mechanism explaining how a human genetic variant in the cytoplasmic tail of DCC may lead to CMM.

INTRODUCTION

In bilaterally symmetric organisms, precise control of midline crossing of axonal tracts is essential for proper coordination of the two sides of the body. During the development of the nervous system, commissural neurons extend their axons across the midline to form connections on the contralateral side in response to attractive guidance cues secreted by midline and other cells (*1*). Netrin-1 is one such conserved guidance cue and acts through its receptor DCC (deleted in colorectal carcinoma), or Frazzled (Fra) in *Drosophila*, to induce attraction toward the midline (*2*). Studies in humans and rodents have shown that the netrin-1–DCC pathway is vital for proper midline connectivity, including normal formation of the corpus callosum and midline crossing of both corticospinal tract axons and spinal commissural axons. Pathogenic variants of DCC cause a spectrum of neurological disorders, including agenesis of the corpus callosum, familial horizontal gaze palsy with progressive scoliosis-2 with impaired intellectual development, and congenital mirror movement (CMM) disorder (*3*–*7*). CMM is characterized by involuntary movements on one side of the body that mimic voluntary movements on the opposite side. The molecular mechanisms of how pathogenic DCC variants lead to CMM, however, are largely unknown.

DCC is thought to respond to netrin-1 and induce axon turning predominantly by modulating the actin cytoskeleton. Considerable experimental evidence supports important roles for the Rho family guanosine triphosphatases Rac1 and Cdc42 and their guanine exchange factors, Src family kinases, and Ena/VASP proteins in DCC-mediated axon attraction in vitro (*8*–*14*). Studies in *Drosophila* and *Caenorhabditis elegans* (*15*–*19*) and, more recently, in rodents and humans (*20*) have shown that some of these effectors are required for netrin-1–DCC–mediated axon guidance in vivo. Yet, how pathogenic variants of DCC perturb interactions with intracellular effectors and affect DCC signaling remains unknown.

Most of the pathogenic variants identified in human DCC that give rise to CMM and agenesis of the corpus callosum are in the extracellular domain of the receptor. These mutations are thought to function by disrupting the binding of DCC to netrin-1, generating truncated proteins, or causing haploinsufficiency of the full-length DCC (*5*). To date, existing pathogenic variants of DCC have not shed light on potential downstream signaling pathways that are important for netrin-1–DCC–dependent axon guidance. Furthermore, few studies have evaluated the pathogenic relevance of any of these variants using physiologically relevant guidance assays.

Through sequencing of *DCC* in a cohort of 80 CMM individuals, we recently identified missense DCC variants associated with CMM (*21*). One of these variants is located in a highly conserved cytoplasmic motif of DCC. This motif fits the consensus sequence of the previously identified WAVE (Wiskott-Aldrich syndrome protein–family verprolin homologous protein) regulatory complex (WRC)–interacting receptor sequence (WIRS), which is found in various membrane receptors and can directly bind to the WRC (*22*), a central regulator of actin cytoskeletal dynamics (*23*). The WRC contains five different subunits—CYFIP1 (cytoplasmic fragile X mental retardation protein–interacting protein 1) or CYFIP2, ABI2 (Abl

[1]Department of Neuroscience, Perelman School of Medicine, University of Pennsylvania, Philadelphia, PA 19104, USA. [2]Montreal Clinical Research Institute (IRCM), Montreal, QC H2W 1R7, Canada. [3]Integrated Program in Neuroscience, McGill University, Montreal, QC H3A 2B4, Canada. [4]Roy J. Carver Department of Biochemistry, Biophysics, and Molecular Biology, Iowa State University, Ames, IA 50011, USA. [5]Department of Anatomy and Cell Biology, Division of Experimental Medicine, McGill University, Montreal, QC H3A 0G4, Canada. [6]McGill University Health Center Research Institute, Montreal, QC H4A 3J1, Canada. [7]Department of Pharmaceutical Sciences, University of Pittsburgh, Pittsburgh, PA 15261, USA. [8]Department of Neurology and Neurosurgery, McGill University, Montreal, QC H3A 2B4, Canada. [9]Department of Pediatrics, Division of Pediatric Neurology, McGill University, Montreal, QC H4A 3J1, Canada. [10]Department of Medicine, University of Montreal, Montreal, QC H3T 1J4, Canada.
*Corresponding author. Email: frederic.charron@ircm.qc.ca (F.C.); gbashaw@pennmedicine.upenn.edu (G.J.B.)
†These authors contributed equally to this work.
‡Present address: Solomon H. Snyder Department of Neuroscience, Johns Hopkins University School of Medicine, Baltimore, MD 21205, USA.

interactor 2), NCKAP1 (also called NAP1; noncatalytic region of tyrosine kinase adaptor protein 1–associated protein 1), HSPC300 (also called BRK1; hematopoietic stem/progenitor cell protein 300), and WAVE1—or their corresponding orthologs and stimulates the actin-related proteins 2 and 3 (Arp2/3) complex to produce branched actin networks (*24*–*26*). That a CMM-associated variant resides in the WIRS motif of DCC suggests that the WRC may play an important role in DCC signaling in axon guidance and that disruption of the DCC-WRC interaction may cause CMM.

Here, we explored whether DCC directly interacts with the WRC and, if so, how this interaction contributes to axon guidance or the pathogenesis of CMM. We found that the DCC-WRC interaction, via the WIRS motif, is an essential and conserved component of netrin-1–dependent DCC/Fra-mediated axon growth and guidance of rat commissural neurons in culture and commissural axon guidance at the *Drosophila* midline in vivo. Our findings reveal insights into the role of DCC variants in the pathogenesis of CMM.

RESULTS

The cytoplasmic domain of DCC directly binds to the WRC

The cytoplasmic domain of human DCC contains a predicted WIRS motif (LRSFAN, amino acids 1342 to 1347) (*22*), which can potentially interact with the WRC. This motif is conserved from humans to *Drosophila* (Fig. 1A). To test whether DCC interacts with the WRC, we coexpressed hemagglutinin (HA)–tagged wild-type DCC (DCC^{WT}) with FLAG-tagged WAVE1, a subunit of the WRC, in human embryonic kidney (HEK) 293 cells. Immunoprecipitation of WAVE1 resulted in the coimmunoprecipitation of DCC^{WT}, suggesting that the WRC interacts with DCC in cells. Similarly, we found that CYFIP2, another subunit of the WRC, also coimmunoprecipitated with DCC (fig. S1). To test whether the interaction between DCC and the WRC is mediated by the cytoplasmic domain of DCC, we coexpressed $DCC^{\Delta cyto}$, a construct lacking the cytoplasmic domain of DCC, with WAVE1. In contrast with DCC^{WT}, $DCC^{\Delta cyto}$ did not coimmunoprecipitate with WAVE1 (Fig. 1, B and C), confirming that

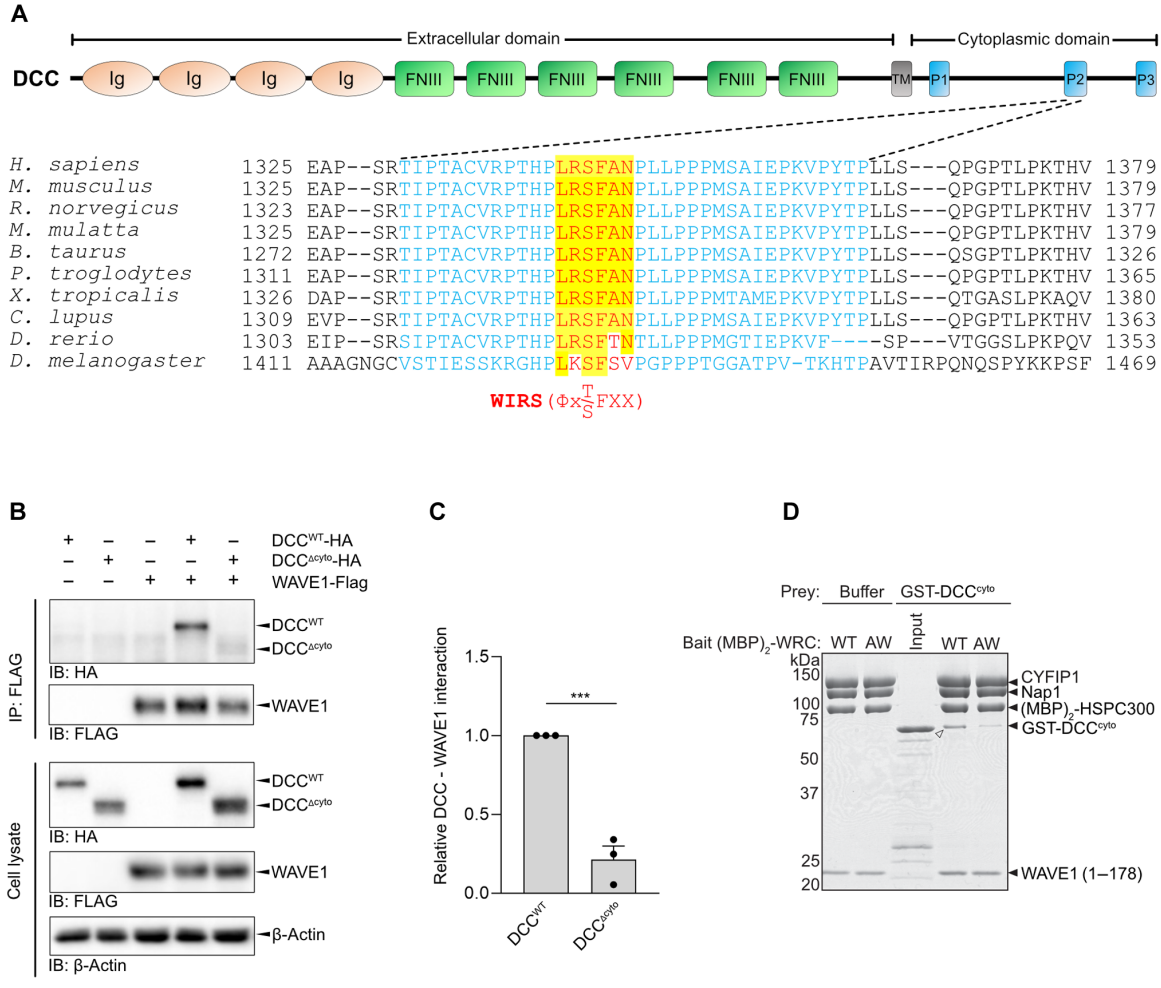

Fig. 1. The WRC interacts with the cytoplasmic domain of DCC. (**A**) Schematic of DCC domains, depicting the WIRS motif (Φ-x-T/S-F-X-X, red) in the P2 domain (cyan), which is conserved across species. Ig, immunoglobin-like C2 domain; FNIII, fibronectin type III–like domain; TM, transmembrane domain; P1 to P3, cytoplasmic conserved domains. (**B** and **C**) HEK 293 cells were transfected with tagged DCC and WAVE1 expression vectors as indicated. The cell lysates were immunoprecipitated (IP) with an antibody to the Flag tag, and the immunoprecipitates were analyzed by Western blotting (IB) with the indicated antibodies. The relative amount (mean ± SEM) of DCC that coimmunoprecipitated with WAVE1 was calculated from $n = 3$ independent experiments. $^{***}P < 0.001$ by unpaired t test. (**D**) Coomassie blue–stained SDS-PAGE gel showing $(MBP)_2$-WRC (WT versus AW mutant, 40 pmol) pulling down GST-DCC^{cyto} (400 pmol) in pull-down buffer containing 120 mM NaCl. White arrowhead indicates the binding signal. Blot is representative of two experiments.

the cytoplasmic domain of DCC is required for its interaction with the WRC.

To test whether the interaction is direct, we performed pull-down assays using purified recombinant proteins and previously established protocols (*22*). In the purified human WRC, the N terminus of the HSPC300 subunit was fused to two maltose-binding proteins, $(MBP)_2$, which can immobilize the WRC to amylose beads to facilitate pull-down assays (*22*). We found that the immobilized $(MBP)_2$-WRC robustly retained the purified, glutathione *S*-transferase (GST)–tagged cytoplasmic domain of DCC (GST-DCC^{cyto}) (Fig. 1D), indicating that the cytoplasmic domain of DCC directly interacts with the WRC. By contrast, this binding signal was substantially reduced when we used a mutant WRC in which the WIRS-binding pocket is disrupted by the point mutations R106A and G110W in the WRC component ABI2 (WRC^{AW}) (*22*). This result suggests that the interaction between the cytoplasmic domain of DCC and the WRC is primarily mediated by the WIRS motif.

A mirror movement DCC variant in the WIRS motif disrupts WRC binding to DCC

Mutations in DCC can cause CMM (*6*). By screening all of the protein coding exons and flanking regions of *DCC* using next-generation sequencing in DNA samples from a cohort of 80 CMM individuals, we recently identified pathogenic variants in DCC associated with CMM (*27*). Among them, one *DCC* variant resulted in a single amino acid change in the WIRS motif (NM_005215, c.4028G > A, p.R1343H) (Figs. 1A and 2A). This variant was extremely rare in controls (alternate allele frequency = 0.000107 in gnomAD 2.1.1), and it was predicted to be disease-causing by in silico tools (Mutationtaster, Polyphen, SIFT); however, according to ACMG (American College of Medical Genetics) criteria, this variant was still considered of unknown significance. Thus, functional studies are needed to confirm the pathogenicity of this variant and to determine whether it results in a loss or gain of DCC function. The R1343 residue is conserved across mammalian species and has only conservative changes in more distant species (Fig. 1A), suggesting that this residue may have an important function.

To test whether the R1343H mutation affects binding to the WRC, we generated DCC constructs containing either the R1343H mutation identified in the CMM case (DCC^{R1343H}) or mutations at the two central amino acids of the WIRS motif (p.SF1344-1345AA, $DCC^{\Delta WIRS}$), which were previously shown to abolish the interaction between other WIRS-containing proteins and the WRC (*22*). We first verified that $DCC^{\Delta WIRS}$ and DCC^{R1343H} do not affect DCC membrane localization or binding to netrin-1. For this, we used a cell surface–binding assay where the binding of $Netrin_{V1.V}$-Fc to DCC^{WT} expressed by COS-7 cells was measured by immunofluorescent detection of cell surface–bound $Netrin_{V1.V}$-Fc (*28*). $Netrin_{V1.V}$-Fc, but not the control Fc, bound to COS-7 cells expressing DCC^{WT} (Fig. 2B). No nonspecific binding due to the Fc fragment or nonspecific signal due to the antibodies used for immunostaining was observed (Fig. 2B and fig. S2A). In COS-7 cells expressing similar levels of $DCC^{\Delta WIRS}$, DCC^{R1343H}, or DCC^{WT} (fig. S2B), there was no significant difference in the amount of $Netrin_{V1.V}$-Fc bound to the cell surface (Fig. 2, B and C). This result confirms that the mutations in the WIRS motif do not affect DCC expression, trafficking, or binding to netrin-1.

After validating that $DCC^{\Delta WIRS}$ and DCC^{R1343H} are expressed on the cell membrane, we tested the effect of these mutations on the interaction with the WRC. Immunoprecipitation of WAVE1 resulted in significantly lower amounts of both $DCC^{\Delta WIRS}$ and DCC^{R1343H} in the coimmunoprecipitates compared with DCC^{WT} (Fig. 2, D and E), indicating that the WIRS motif is important for the interaction between DCC and the WRC. We further validated the effect of $DCC^{\Delta WIRS}$ and DCC^{R1343H} in disrupting WRC binding using pull-down assays with purified recombinant proteins. Compared with GST-$DCC^{WT\text{-}cyto}$, the pull-down signals of GST-$DCC^{\Delta WIRS\text{-}cyto}$ and GST-$DCC^{R1343H\text{-}cyto}$ by $(MBP)_2$-WRC were both significantly reduced (Fig. 2, F and G). This result demonstrates that the direct interaction between DCC and the WRC requires the WIRS motif and that the CMM-associated DCC^{R1343H} mutation disrupts this interaction.

The DCC WIRS motif is required for netrin-1–dependent directional axon outgrowth

Given that the DCC^{R1343H} variant has a reduced interaction with the WRC and is present in a CMM individual, we hypothesized that the DCC WIRS motif has an important function in axon guidance. To test this hypothesis, we used rodent spinal cord commissural neurons to determine how the DCC WIRS contributes to netrin-1–DCC signaling in axon guidance. Spinal commissural neurons express *Dcc* and rely on netrin-1–DCC signaling to guide their axons to the ventral midline (*28*–*32*). We first tested whether the biochemical interaction that we observed between DCC and the WRC also occurs between endogenous proteins in commissural neurons using a proximity ligation assay (PLA). PLA produces immunofluorescence signals when the proteins of interest are in close proximity (<40 nm), indicating a high likelihood of physical interaction. We performed PLA between DCC and the CYFIP2 subunit of the WRC because we have CYFIP2-specific antibodies suitable for immunofluorescence detection (*33*). Consistent with our biochemical results, we detected PLA signals between CYFIP2 and DCC in control commissural neurons that were mock-stimulated with bovine serum albumin (BSA) (Fig. 3A), indicating a basal level of interaction between CYFIP2 and DCC in the growth cone. Stimulating the neurons with netrin-1 for 5 or 30 min significantly reduced PLA signals in the growth cone (Fig. 3, A to C), suggesting that netrin-1 stimulation releases the WRC from DCC.

To examine how the WIRS mutants, including $DCC^{\Delta WIRS}$ and DCC^{R1343H}, affect netrin-1–mediated directional axon growth, we turned to mouse dorsal spinal cord explants. Dorsal spinal cord explants were electroporated with red fluorescent protein (RFP) and the DCC variants and cultured next to mock 293T cell aggregates or aggregates expressing netrin-1 (Fig. 3D and fig. S3D). The amount of *Ntn1* DNA (encoding netrin-1) used for transfection of 293T cells and the stage of the embryos [embryonic day (E12) rather than E11 when axons are actively crossing the floor plate] were selected so as to elicit a milder netrin-1 response and allow for more sensitive detection of phenotypes upon the expression of DCC variants. We quantified the response to netrin-1 by measuring the ratio of axon outgrowth extending from the side of the explant closest to the aggregate (proximal side) versus the far side (distal side). To ensure that each of these HA-tagged DCC variants was expressed at similar levels, we quantified the HA expression in dissociated spinal commissural neuron cultures prepared from electroporated spinal cords. Immunostaining for HA showed comparable levels of each DCC variant in dissociated neurons (fig. S3, A and B). Coexpression of RFP was used as a measure of electroporation efficiency because of poor penetration of the anti-HA antibody in collagen-embedded explants (fig. S3C).

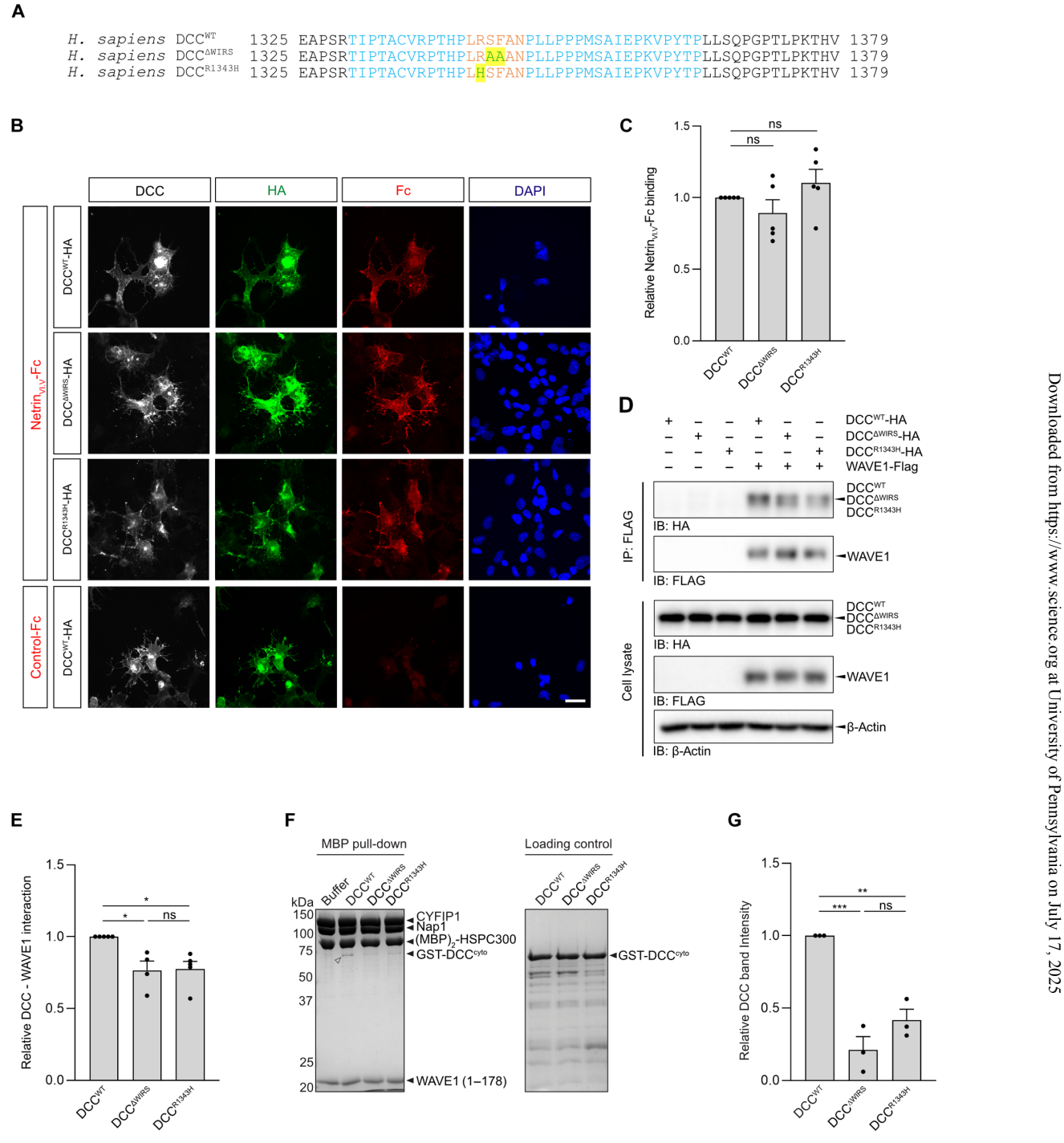

Fig. 2. A mirror movement–associated variant in the WIRS motif of DCC disrupts binding to the WRC. (**A**) Amino acid alignment of human DCC^{WT}, DCC$^{\Delta WIRS}$ (p.SF1344-1345AA), and DCC^{R1343H} (p.R1343H). The mutated residues are highlighted. (**B** and **C**) COS7 cells transfected with the DCC^{WT}, DCC$^{\Delta WIRS}$, and DCC^{R1343H} expression vectors were incubated with Netrin$_{VI,V}$-Fc or control-Fc conditioned medium. Cells were immunostained with antibodies to DCC, HA, and Fc. Scale bar, 40 μm. Images are representative of five experiments. The relative amount of Netrin$_{VI,V}$-Fc binding to the cell surface, quantified from the immunofluorescence images as depicted in (B), is shown in (C). Data are means ± SEM of $n = 5$ experiments, 20 to 25 cells per condition per experiment, analyzed by one-way ANOVA with Dunnett's multiple comparisons posttest; ns, not significant. (**D** and **E**) HEK 293 cells were transfected with tagged DCC and WAVE1 expression vectors as indicated. The cell lysates were immunoprecipitated (IP) with an antibody to Flag, and the immunoprecipitates were analyzed by Western blotting (IB) with the indicated antibodies. The relative amount (means ± SEM) of the DCC variants that coimmunoprecipitated with WAVE1 was calculated from $n = 5$ independent experiments. *$P < 0.05$ by one-way ANOVA with Tukey's multiple comparisons posttest. (**F**) Coomassie blue–stained SDS-PAGE gels showing $(MBP)_2$-WRC (60 pmol) pulling down the indicated GST-DCC^{cyto} constructs (400 pmol) in a pull-down buffer containing 150 mM NaCl. White arrowhead indicates the binding signal. (**G**) Quantification (means ± SEM) of relative GST-DCC^{cyto} band intensities from the $(MBP)_2$-WRC pull-down experiments in (F). $n = 3$ experiments. Signals were normalized to the DCC$^{WT\text{-}cyto}$ sample. **$P < 0.005$ and ***$P < 0.001$ by ANOVA with Tukey's posttest; ns, not significant.

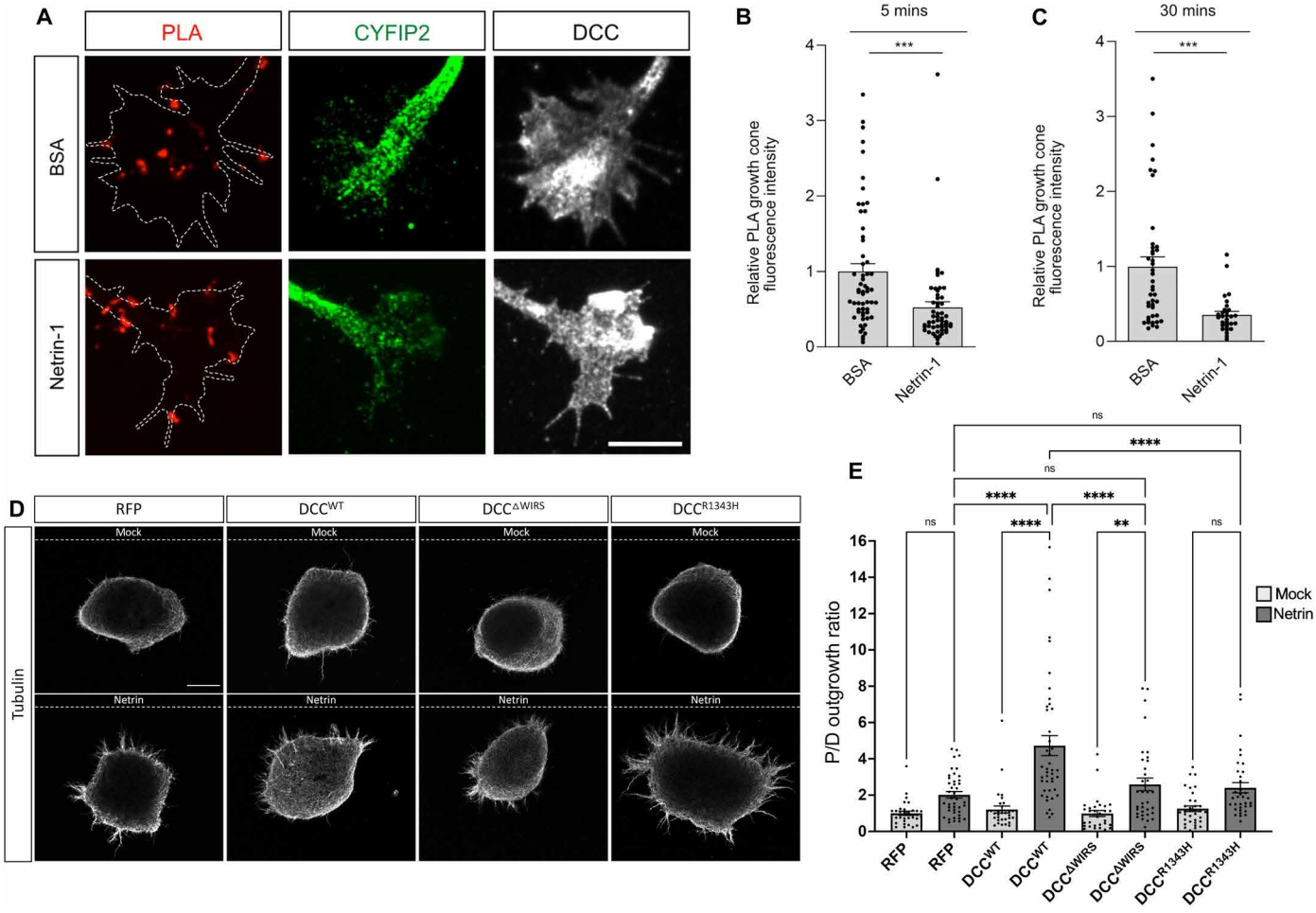

Fig. 3. The DCC WIRS motif is required for netrin-dependent directional axon growth. (**A** to **C**) Dissociated commissural neurons were treated with BSA (0.1 μg/ml) or netrin-1 for 5 min and then fixed. The PLA assay was performed for DCC and CYFIP2. Scale bar, 10 μm. The mean (±SEM) intensity of the PLA signal in the growth cone after 5 min (B) and 30 min (C) of netrin-1 stimulation was assessed in $n = 3$ (B) and $n = 2$ (C) independent experiments, with ≥9 growth cones per condition per experiment, and normalized to the mean signal in the BSA condition. ***$P < 0.001$ by t test. (**D** and **E**) E12 dorsal spinal cord explants, electroporated with either RFP, DCC^{WT}, DCC$^{\Delta WIRS}$, or DCC^{R1343H} and cultured next to a mock or netrin-expressing cell aggregate, were labeled with antibody to β-tubulin to visualize axon outgrowth. Dotted lines indicate the position of either the mock or the netrin-expressing cell aggregate. Scale bar, 100 μm. Quantification of the proximal/distal outgrowth ratios for explants cultured next to mock cell aggregates (white) or netrin-expressing cell aggregates (gray). Data are means ± SEM of $n = 31$, 42, 43, 32, 34, 35, 35, and 31 explants from two independent experiments. **$P < 0.01$ and ****$P < 0.0001$ by one-way ANOVA with Tukey's multiple comparisons test.

Explants cultured next to mock cell aggregates that did not express netrin-1 showed little to no growth that was uniform on both sides of the explant (Fig. 3, D and E). Explants electroporated with RFP alone and cultured next to netrin-1–expressing aggregates showed slightly more growth on the proximal side compared with the distal side, resulting in a small but not statistically significant increase in the proximal/distal outgrowth ratio (Fig. 3, D and E). Consistent with the role of DCC in netrin-1–mediated axon outgrowth, explants electroporated with DCC^{WT} showed an enhanced response to netrin-1, with significantly more growth on the proximal side and a significantly greater proximal/distal outgrowth ratio compared with the RFP-electroporated explants cultured with netrin-1 aggregates (Fig. 3, D and E). In contrast, explants electroporated with DCC$^{\Delta WIRS}$ and cultured with netrin-1 aggregates did not have a significantly different proximal/distal outgrowth ratio compared to that observed for RFP-electroporated control explants cultured with netrin-1 aggregates (Fig. 3, D and E). This finding indicates that DCC$^{\Delta WIRS}$ is unable to induce directional axon growth in response to netrin-1. Similarly, explants electroporated with DCC^{R1343H} also failed to show an enhanced response to netrin-1 and had a proximal/distal outgrowth ratio comparable to that of controls cultured with netrin-1 aggregates (Fig. 3, D and E). The values of the proximal/distal ratios for both DCC variants were similar to each other and not significantly different from the control RFP-electroporated explants across the netrin-1 conditions. The proximal/distal ratios for both variants when cultured with netrin-1 aggregates were significantly lower than those for DCC^{WT}, reflecting a marked reduction in responsiveness to netrin. Thus, mutations in the DCC WIRS motif lead to a loss of DCC-mediated directional axon outgrowth in response to netrin-1.

The DCC WIRS motif is required for netrin-1–mediated axon guidance

Having established that the DCC WIRS motif is important for netrin-1–DCC–mediated directional axon outgrowth, we next tested

whether the DCC WIRS motif is also required for netrin-1–mediated commissural axon turning in vitro using a DCC knockdown/reexpression strategy. Using small interfering RNA (siRNA) against rat *Dcc*, we were able to reduce endogenous DCC abundance by ~50% in dissociated rat commissural neurons (fig. S4, A and B). To assess netrin-1–mediated axon turning, we used an in vitro axon turning assay in which cultured rat commissural neurons were exposed to a netrin-1 gradient in a Dunn chamber. The turning of the axons toward the gradient was then imaged, and the angle turned was defined as the angle between the initial and final orientation of the axon, with positive turning angles representing attraction toward the gradient (*34*). When commissural neurons electroporated with control scrambled siRNA were exposed to a netrin-1 gradient, their axons were attracted toward the higher concentration of netrin-1, and the angle turned showed a significant bias toward positive angles. In contrast, *Dcc* knockdown inhibited the ability of axons to turn toward the netrin-1 gradient; no net turning occurred, and the turning angle varied around 0 (Fig. 4, A to C).

We next sought to rescue the effect of *Dcc* knockdown by expressing human DCC (DCC^{WT}), which is not targeted by the rat *Dcc* siRNA. Expression of DCC^{WT}, but not the empty vector control (fig. S4C), in DCC knockdown neurons completely rescued netrin-1–mediated axon attraction, with the axons turning equally well toward netrin-1 compared to control axons electroporated with scrambled siRNA/empty vector (Fig. 4, A to C). This demonstrates that the effect of *Dcc* knockdown on inhibiting netrin-1–mediated axon turning is not due to off-target effects of the siRNA and that expression of wild-type DCC is sufficient to mediate axon turning to netrin-1. In contrast, expression of the DCC WIRS variants, $DCC^{\Delta WIRS}$ or DCC^{R1343H} (fig. S4C), did not rescue netrin-1–mediated attraction in DCC-knockdown neurons, and these axons failed to turn toward the netrin-1 gradient (Fig. 4, A to C). These results indicate that mutating the WIRS motif is sufficient to disrupt netrin-1–mediated attraction and that DCC^{R1343H} is a loss-of-function variant. There was no significant difference in the speed of axon growth under these conditions (Fig. 4D), suggesting that the lack of turning in DCC-knockdown or $DCC^{\Delta WIRS}$- or DCC^{R1343H}-expressing neurons was not due to a reduction in axon growth. Together, our data demonstrate that the DCC WIRS motif is required for netrin-1–mediated axon attraction.

Fra directly interacts with the WRC through the WIRS motif in the cytoplasmic domain

The WIRS motif in the cytoplasmic domain DCC is conserved in its *Drosophila* ortholog, Fra (Fig. 1A). To determine whether the interaction we observed between human DCC and the WRC is conserved, we tested the binding between Fra and the *Drosophila* WRC. We first performed a series of coimmunoprecipitation experiments using cultured insect cells and *Drosophila* embryonic lysates. By expressing tagged constructs of Fra and the HSPC300 subunit of the WRC in *Drosophila* $S2R^+$ cells, we found that Fra coimmunoprecipitated with HSPC300, indicating that Fra interacts with the WRC in *Drosophila* cells (Fig. 5A). Deleting the P2 domain ($Fra^{\Delta P2}$), which contains the WIRS motif, or mutating the central two amino acids of the WIRS motif ($Fra^{\Delta WIRS}$), significantly reduced binding (Fig. 5, A and B), highlighting the importance of the WIRS motif for the interaction between Fra and the WRC. To further test whether Fra and the WRC also interact in vivo, we performed coimmunoprecipitation experiments from *Drosophila* embryonic lysates. We used the pan-neuronal *elav-Gal4* driver to direct neuron-specific expression of green fluorescent protein (GFP)–tagged HSPC300 and Myc-tagged Fra. Like the results from cultured $S2R^+$ cells, Fra^{WT} immunoprecipitated with HSPC300 in embryonic lysates (Fig. 5C), whereas both $Fra^{\Delta WIRS}$ and $Fra^{\Delta P2}$ showed a significant reduction in binding to the WRC (Fig. 5, C and D). Collectively, our results indicate that Fra interacts with the *Drosophila* WRC in a WIRS-dependent manner.

We next used pull-down assays with purified recombinant proteins to test whether the Fra-WRC interaction is direct and whether it depends on the WIRS motif. GST-tagged $Fra^{WT\text{-}cyto}$, but not GST-$Fra^{\Delta WIRS\text{-}cyto}$, robustly bound to $(MBP)_2$-tagged WRCs from both humans and *Drosophila* (Fig. 5, E and F). Mutating the WIRS-binding pocket on the WRC ($WRC^{\Delta W}$) abolished the binding (Fig. 5E) (*22*). Consistently, addition of a synthesized WIRS peptide derived from human protocadherin-10 (PCDH10) (*22*), but not a mutant WIRS peptide, effectively blocked the binding (Fig. 5F). Together, these results confirm that, like DCC (Fig. 2, F and G), the cytoplasmic domain of Fra^{WT} directly interacts with the WRC through the conserved WIRS motif. Therefore, it is likely that the DCC/Fra WIRS-WRC interaction has a conserved function across different species.

The Fra WIRS motif is required for commissural axon guidance at the *Drosophila* midline

Our data showing that the DCC WIRS motif is required for netrin-1–mediated commissural axon guidance in vitro strongly suggest that the WIRS motif and the WRC are required for netrin-1–DCC–dependent axon guidance in vivo. To evaluate the significance of the DCC/Fra WIRS motif and the WRC in commissural axon guidance in vivo, we decided to use the developing nerve cord in *Drosophila* as a model system. This system is ideal to assess functional axon guidance requirements of the WRC because, unlike mammalian systems, the *Drosophila* genome encodes only a single gene for each of the five components of the WRC. In addition, WRC members are enriched in the *Drosophila* ventral nerve cord during embryonic stages when midline crossing occurs (*35*, *36*). To evaluate the importance of the Fra WIRS motif in vivo, we assessed the ability of $Fra^{\Delta WIRS}$ to rescue the axon crossing defects present in the eagle neurons of *fra* mutants. Eagle neurons are a subset of commissural neurons and consist of an EG population, which projects into the anterior commissure of each segment, and an EW population, which projects into the posterior commissure (Fig. 6A). In *fra3* mutants, 56% of EW axons fail to cross the midline (Fig. 6, A and B), and horseradish peroxidase (HRP) immunostaining reveals frequent missing commissures and breaks in longitudinal tracts (Fig. 6B). Re-expressing Fra^{WT} specifically in eagle neurons almost completely rescued the EW noncrossing defects, with only 13% of segments still showing defects (Fig. 6, A and B). Because this transgene was only expressed in eagle neurons, we still observed *fra* mutant phenotypes in the axon scaffold with frequent missing and/or thin commissures (Fig. 6A). In contrast with Fra^{WT}, reexpression of $Fra^{\Delta WIRS}$ failed to rescue the *fra* mutant phenotype, with 42% of EW axons still failing to cross (Fig. 6, A and B). Together, these results show that Fra without a functional WIRS motif is unable to restore attractive signaling and that the WIRS motif is required for Fra-attractive signaling at the *Drosophila* midline in vivo.

The WRC genetically interacts with the Fra pathway in the *Drosophila* nerve cord

Given that the WIRS motif serves as an interaction site for the WRC, we next investigated whether the WRC functions in the Fra pathway

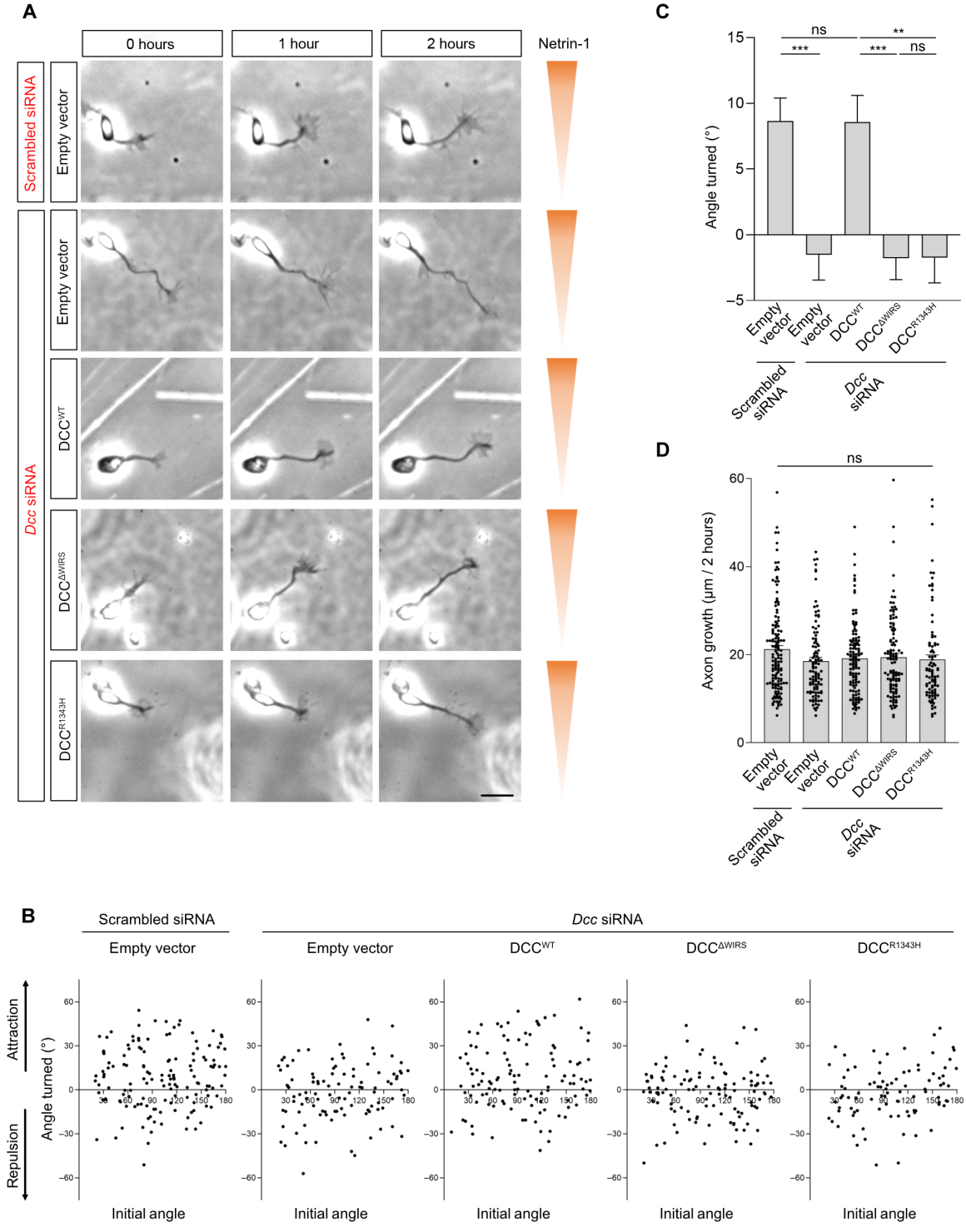

Fig. 4. The DCC WIRS motif is required for netrin-1–mediated axon guidance. (**A**) Time-lapse imaging of commissural axons growing in a netrin-1 gradient in a Dunn chamber and expressing the indicated DCC constructs and control scrambled or *Dcc* siRNA. The netrin-1 gradient increases along the *y* axis. Scale bar, 20 µm. (**B**) Scatter plot of the angle turned versus the initial angle (defined as the angle between the initial orientation of the axon and the gradient) for commissural axons described in (A) from $n = 3$ independent experiments. (**C**) The mean angle turned (±SEM) for commissural axons in the indicated conditions, as in (A). $^{***}P < 0.001$, $^{**}P < 0.01$, and ns, not significant by one-way ANOVA with Tukey's post hoc test. (**D**) Axon growth (means ± SEM) over 2 hours from assay described in (A). Difference was not significant; $P = 0.3266$ by one-way ANOVA.

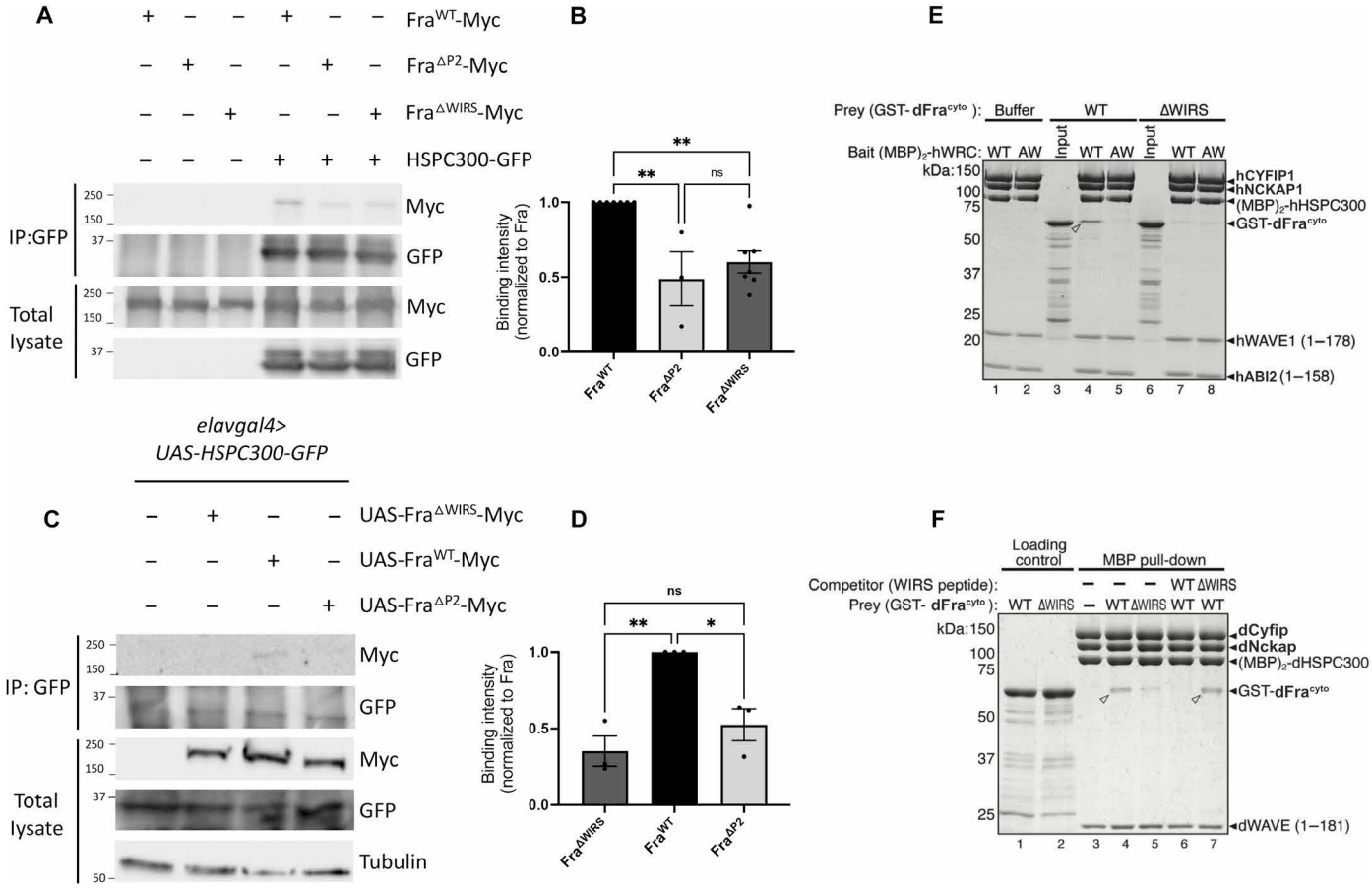

Fig. 5. Fra directly interacts with the WRC through the WIRS motif. (**A** and **B**) *Drosophila* S2R$^+$ cell lysates coexpressing HSPC300-GFP with either Fra^{WT}-Myc, Fra$^{\Delta P2}$-Myc, or Fra$^{\Delta WIRS}$-Myc were immunoprecipitated with an antibody to GFP. Quantitation of the band intensities of the Myc-tagged Fra variants in the immunoprecipitates normalized to Fra^{WT}-Myc. Data were further normalized to the lysate levels of the Fra variants and HSPC300 levels in the immunoprecipitates. Error bars represent SEM. $n = 7$ experiments for Fra$^{\Delta WIRS}$ and $n = 3$ for Fra$^{\Delta P2}$ (B). $^{**}P < 0.01$ and ns, not significant by one-way ANOVA with Tukey's multiple comparisons test. (**C** and **D**) Lysates from *Drosophila* embryos with *elavGal4*-driven neuronal expression of HSPC300-GFP with Fra$^{\Delta WIRS}$-Myc, Fra^{WT}-Myc, or Fra$^{\Delta P2}$-Myc were immunoprecipitated with an antibody to GFP. Analysis as detailed for (B), from $n = 3$ experiments, and $^{*}P < 0.05$. (**E**) Coomassie blue–stained SDS-PAGE gel showing $(MBP)_2$-tagged human WRC (40 pmol, WT versus AW mutant) pulling down the indicated GST-Fra^{cyto} constructs (400 pmol) in a pull-down buffer containing 100 mM NaCl. (**F**) Coomassie blue–stained SDS-PAGE gel showing $(MBP)_2$-tagged *Drosophila* WRC (40 pmol) pulling down the indicated GST-Fra^{cyto} constructs (400 pmol) in a pull-down buffer containing 50 mM NaCl, in the absence or presence of chemically synthesized WIRS-containing peptides (0.25 μM, WT versus ΔWIRS mutant) as a competitor. In (E) and (F), white arrowheads indicate binding signals. Gel images are representative of two experiments, except for lanes 6 and 7 in (F), which were performed once.

at the *Drosophila* midline. First, to determine whether the WRC is important for midline crossing, we used an Fra$^{\Delta cyto}$-sensitized background in which commissural eagle neurons express a truncated Fra receptor (Fra$^{\Delta cyto}$) lacking its cytoplasmic domain and that functions as a dominant negative (*37*). This manipulation results in some axons failing to cross the midline and constitutes a sensitized background in which we can detect positive or negative regulators of midline crossing. Expressing one copy of *fra*$^{\Delta cyto}$ in eagle neurons resulted in 33% of EW neurons failing to cross the midline (fig. S5, A and B). CYFIP is a member of the WRC, and *cyfip* mutants showed no noncrossing defects in eagle neurons (Fig. 6, A and C). In *cyfip* mutants along with all other WRC mutants, significant amounts of protein still remain because of maternal deposition (*36*, *38*), which is likely why they showed no defects on their own. However, removing one copy of *cyfip* in this Fra$^{\Delta cyto}$ background significantly enhanced EW noncrossing defects to 49% (fig. S5, A and B). SCAR (the *Drosophila* WAVE ortholog) and HSPC300 are two other subunits of the WRC, and removing one copy of *scar* resulted in a similar enhancement of EW noncrossing defects to 46%, whereas removing one copy of *hspc300* had no effect (fig. S5, A and B). Together, these results suggest a role for the WRC in promoting midline crossing.

To further assess whether the WRC functions in the Fra pathway to regulate midline crossing, we examined genetic interactions between *cyfip* and *fra* using a *fra* hypomorphic background. Whereas *fra*^{4} is an amorphic allele, *fra*^{6} is a hypomorphic allele (*39*, *40*), and *fra*^{4}/*fra*^{6} hypomorphic *fra* mutants showed a relatively mild noncrossing phenotype in which EW axons failed to cross in 18% of nerve cord segments (Fig. 6, A and C). HRP immunostaining labeled all central nervous system (CNS) axons and showed infrequent breaks in longitudinal tracts and thinning of commissures in these mutants (Fig. 6A). Whereas *cyfip* mutants on their own had no noncrossing defects, the

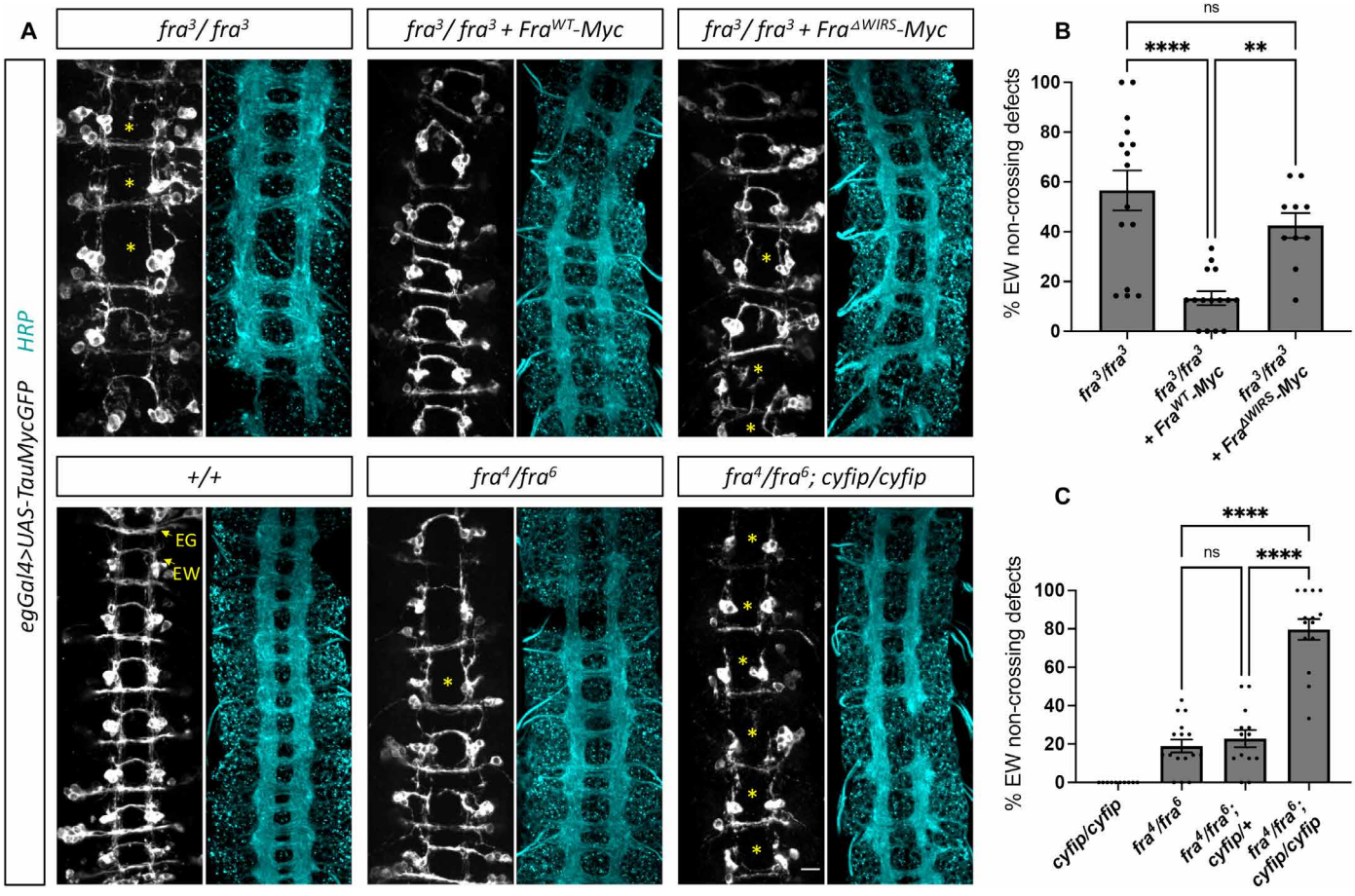

Fig. 6. The WRC genetically interacts with the *fra* pathway in the *Drosophila* nerve cord. (**A**) Assessment of EW commissural crossing defects in stage 16 *Drosophila* embryos carrying *egGal4* and *UAS-TauMycGFP* transgenes stained with anti-GFP (grayscale), which labels cell bodies and axons of the eagle neurons, or anti-HRP (cyan), which labels all CNS axons. Scale bar, 10 μm. (**B** and **C**) Quantitation of the percentage of segments in which EW axons fail to cross the midline. Data are means ± SEM, number of embryos $n = 15$, 15, and 10, respectively, in (B), and $n = 10$, 16, 13, and 14, respectively, in (C). $^{**}P < 0.01$, $^{****}P < 0.0001$, and ns, not significant by one-way ANOVA with Tukey's multiple comparisons test.

removal of *cyfip* in these *fra* hypomorphic mutants resulted in a substantial enhancement of the noncrossing defects, with EW axons failing to cross in almost 80% of segments (Fig. 6, A and C). HRP immunostaining also revealed a more severe phenotype with frequent missing commissures and longitudinal breaks in the axon scaffold (Fig. 6A). Although this strong genetic interaction does not exclude the possibility that the WRC functions in additional pathways that promote midline crossing, it shows that one function of the WRC is in the Fra pathway to mediate attraction at the *Drosophila* midline. To directly assess whether the WRC functions exclusively in the *fra* pathway or whether it also acts outside of the *fra* pathway to control axon guidance or other aspects of embryonic development, we generated double mutants between *cyfip* mutants and *fra* null mutations. Unfortunately, these embryos had severe developmental disruptions, and they survived at non-Mendelian ratios, rarely reaching stage 13, a stage that is too early for us to evaluate axon guidance (fig. S6). These data suggest that Cyfip and the WRC also act in additional Fra-independent pathways. Given the fundamental roles for the WRC in regulating the actin cytoskeleton, we think it would be quite unexpected should its embryonic functions be restricted to one particular signaling pathway.

DCC^{R1343H} and DCC$^{\Delta WIRS}$ have reduced signaling activity in vivo

So far, we found that the interaction between DCC and the WRC (Figs. 1 and 2) is conserved in *Drosophila* (Fig. 5), that the DCC-WRC interaction is required for netrin-1–mediated axon guidance in rodent and human commissural neurons in vitro (Fig. 4), and that the WIRS motif (and Fra-WRC interaction) is likewise required for Fra-attractive signaling at the *Drosophila* midline in vivo (Fig. 6). Therefore, the requirement of the DCC-WRC interaction in axon guidance appears to be conserved across species. Consequently, we predicted that DCC^{R1343H} and DCC$^{\Delta WIRS}$ would impair commissural axon guidance in vivo and that this impairment may contribute to the pathogenic mechanism underlying mirror movements.

To test this hypothesis, we first generated a set of DCC transgenes for GAL4–upstream activating sequence (UAS) expression in *Drosophila*. Reasoning that DCC would likely not function as well as the native *fra* gene in *Drosophila*, we opted to generate DCC transgenes with 10 UAS-binding sites (10X-UAS) to optimize expression. Using these transgenes, we performed a series of rescue experiments to determine whether expression of human DCC transgenes could

restore midline crossing in embryos carrying mutations for *fra* (fig. S7, A to D). Our rescue assay in *fra3* mutants was initially performed using 5X-UAS inserts of the Fra^{WT} and $Fra^{\Delta WIRS}$ transgenes (Fig. 6A); therefore, to allow us to directly compare Fra and DCC receptor activities, we generated a second set of 10X-UAS–Fra transgenes and conducted rescue experiments in parallel for Fra and DCC. 10X-UAS–Fra^{WT} completely rescued the *fra* mutant, whereas 10X-UAS–$Fra^{\Delta WIRS}$ conferred a partial rescue, with 10X-UAS–$Fra^{\Delta WIRS}$ axons showing significantly more EW crossing defects than 10X-UAS–Fra^{WT} axons (fig. S7, A and B). We found that all 10X-UAS–DCC transgenes that we tested completely rescued the Fra mutant phenotype, with no significant difference in the ability of $DCC^{\Delta WIRS}$ and DCC^{R1343H} to rescue the EW axon crossing defects compared to DCC^{WT} (fig. S7, A and C). This suggests that $DCC^{\Delta WIRS}$ and DCC^{R1343H} have a similar activity to DCC^{WT} when expressed at 10X-UAS, but it is possible that lower expression of the variants would reveal differences in their ability to rescue the *fra* mutant phenotype. Supporting this, the 10X-UAS–$Fra^{\Delta WIRS}$ partially rescued the *fra* mutant phenotype, whereas 5X-UAS–$Fra^{\Delta WIRS}$ failed to rescue, most likely reflecting the increased expression levels from the 10X transgenes leading to reduced sensitivity in detecting differences in receptor activity (*35*). When we compared the rescue ability of DCC and Fra, the DCC transgenes consistently provided better rescue of the *fra* mutant phenotypes. This is particularly notable when we compared the ability of the ΔWIRS variants to rescue because the $DCC^{\Delta WIRS}$ transgene was significantly better at rescuing than was $Fra^{\Delta WIRS}$ (fig. S7, A and C). That $DCC^{\Delta WIRS}$ had greater signaling activity than the analogous $Fra^{\Delta WIRS}$ may be due to DCC, but not Fra, interacting with the WRC through an additional non-WIRS–binding site. Supporting this, our biochemical observations (Figs. 2 and 5) showed that the loss of interaction between DCC/Fra and the WRC was milder with $DCC^{\Delta WIRS}$ and more complete with $Fra^{\Delta WIRS}$, suggesting that a second WRC-binding site might be present in $DCC^{\Delta WIRS}$.

As an alternative strategy to evaluate the relative activity of DCC^{R1343H} and $DCC^{\Delta WIRS}$, we performed a series of gain-of-function experiments in a subset of ipsilateral neurons. We first established this assay with Fra. In wild-type ($^{+/+}$) embryos, the apterous (ap) population of ipsilateral axons never crossed the midline and expressed little to no Fra (Fig. 7A) (*41*). Overexpression of 10X-UAS Fra^{WT} in ap axons resulted in a strong gain-of-function phenotype where 68% of ap axons ectopically crossed the midline (Fig. 7, A and B). In contrast, overexpression of either $Fra^{\Delta P2}$ or $Fra^{\Delta WIRS}$ resulted in a significantly weaker gain-of-function phenotype, with ~48% of ap axons ectopically crossing the midline (Fig. 7, A and B). The reduction in the gain-of-function phenotype observed with $Fra^{\Delta P2}$ and

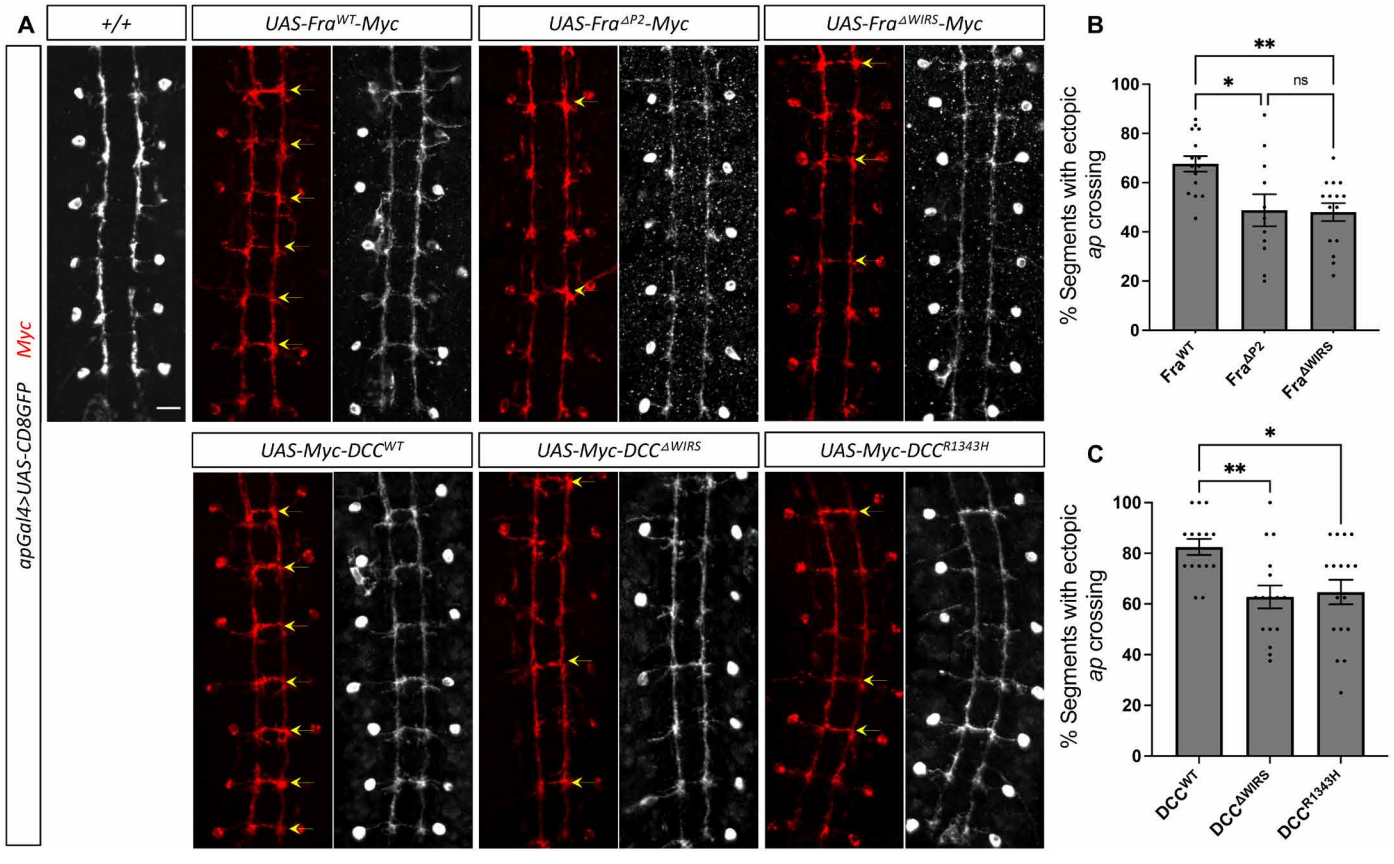

Fig. 7. DCC^{R1343H} and $DCC^{\Delta WIRS}$ have reduced signaling activity in vivo. (**A**) Assessment of ectopic crossing in stage 16 *Drosophila* embryos carrying *apGal4* and *UAS-CD8GFP* transgenes stained with anti-GFP, which labels the ap cell bodies and axons, or anti-Myc, which labels the corresponding Myc-tagged transgenes. Scale bar, 10 μm. (**B** and **C**) Quantitation of the percentage of segments in which ap axons ectopically cross the midline. Data are means ± SEM. Number of embryos $n = 15$, 11, and 15, respectively, in (B) and $n = 15$, 16, and 17, respectively, in (C). $^*P < 0.05$, $^{**}P < 0.01$, and ns, not significant by one-way ANOVA with Tukey's multiple comparisons test.

$Fra^{\Delta WIRS}$ was not due to differences in expression levels of Fra^{WT}, $Fra^{\Delta P2}$, and $Fra^{\Delta WIRS}$ because immunostaining for Myc showed comparable levels of expression of all three transgenes (fig. S8, A and B). Thus, our gain-of-function assay with Fra variants demonstrated that disrupting the WIRS motif affected Fra's ability to induce ectopic attraction, consistent with the WIRS motif being required for Fra-attractive signaling at the *Drosophila* midline.

Next, we examined the consequences of the DCC WIRS mutations in vivo by expressing the DCC variants in the *Drosophila* nerve cord and examining their ability to induce ectopic attraction toward the midline. We have previously shown that DCC can signal in response to *Drosophila* netrin-1 and induce ectopic crossing at the midline when introduced into the ap population of ipsilateral axons (*42*). Overexpressing DCC in these axons results in a strong gain-of-function phenotype where more than 80% of ap axons ectopically crossed the midline (Fig. 7, A and C). In contrast, overexpressing $DCC^{\Delta WIRS}$ or DCC^{R1343H} (Fig. 7, A and C) resulted in significantly weaker gain-of-function phenotypes, with approximately 62% of ap axons ectopically crossing the midline (Fig. 7, A and C). All transgenes were tagged with Myc, and immunostaining showed comparable levels of expression of all transgenes (fig. S8, C and D), indicating that the reduction in the gain-of-function phenotype was not due to differences in expression levels of DCC^{WT}, $DCC^{\Delta WIRS}$, and DCC^{R1343H}. These results show that mutations in the DCC WIRS motif impair DCC's ability to induce ectopic attraction in vivo. This is consistent with our demonstration that DCC^{R1343H} cannot rescue commissural axon attraction to netrin-1 when DCC is knocked down, indicating that DCC^{R1343H} is a loss-of-function mutation. Our finding that disrupting the WIRS motif ($DCC^{\Delta WIRS}$) has a similar effect to DCC^{R1343H} supports the conclusion that DCC^{R1343H} is likely pathogenic by disrupting the interaction of the WIRS motif with the WRC.

DISCUSSION

We have documented an essential role for the WIRS-WRC interaction in netrin-1–mediated DCC/Fra signaling. The functional significance of this interaction is underscored by the presence of a mutation in the WIRS motif, DCC^{R1343H}, found in a CMM individual (*27*). This pathogenic variant disrupts DCC guidance function in mammalian neurons and in flies, supporting the idea that DCC^{R1343H} causes CMM by disrupting netrin-1–DCC signaling and axon guidance.

The WIRS motif is present in several axon guidance receptors, including the repulsive guidance receptor, Robo, and our laboratory recently identified the WRC as an important downstream effector of Robo signaling (*35*). Some important questions that arise are how the WIRS-WRC interaction is regulated in different pathways and how the WRC functions downstream of DCC and Robo to achieve distinct and opposing outputs. One possibility might be the spatial segregation of WRC activation. We previously demonstrated that addition of slit, the ligand for Robo, increased the interaction between the WRC and Robo (*35*). In contrast, we found here that addition of netrin-1 released the WRC from DCC in growth cones of commissural neurons. This difference in WRC response to ligand might be due to a difference in how the WRC acts in attraction versus repulsion. Given the positive role for the WRC in DCC/Fra signaling, we speculate that DCC might act as a scaffold, bringing active Rac1 and the WRC in proximity to locally concentrate active WRC. Rac1, an important activator of the WRC (*43*, *44*), has previously been implicated downstream of DCC and could serve to activate the WRC at DCC-WRC interaction sites (*9*, *45*, *46*). DCC is rapidly endocytosed from the plasma membrane after netrin-1 stimulation (*47*–*49*), and the release of active WRC upon netrin-1 binding before DCC endocytosis could enable retention of the complex at the growth cone membrane where enhanced actin polymerization is important for driving growth cone advancement and turning.

Recent reports have shed light on an inhibitory effect of actin polymerization on growth, whereby the accumulation of actin in the central region of the growth cone prevents microtubules from extending into the periphery to induce axon growth (*50*). It is tempting to hypothesize that downstream of DCC, the WRC is activated and concentrated at the plasma membrane to induce the formation of branched actin filaments, which propel the growth cone forward. In contrast, WRC activation downstream of Robo may occur deeper within the growth cone, such as in the central region, where the resulting increase in actin filaments serves as a barrier to microtubules and restricts axon growth. Robo is endocytosed in response to slit (*51*), and this is required for its downstream activation of Rac1. Because Rac1 activates the WRC, it is likely that WRC activation also occurs on endosomes, rather than at the plasma membrane, and that these endosomes may be positioned in deeper regions of the growth cone. Consistently, super-resolution imaging of Robo1 distribution in commissural axon growth cones reveals that Robo1 accumulates more centrally in the growth cone and is detected at lower levels at the leading edge (*52*). Alternatively, WRC activation and actin polymerization may occur at the plasma membrane downstream of all axon guidance receptors and could represent a generalized mechanism for initial gradient sensing upon guidance cue detection. In support of this, dorsal root ganglion neurons initially extend filopodia toward a source of slit before retracting (*53*).

Adding increased complexity to actin regulatory pathways, the WRC can also bind to neuronal receptors in a WIRS-independent manner (*54*–*57*). Our biochemical data show that the interaction between Fra and the WRC is primarily through its WIRS motif. However, the interaction between DCC and the WRC is not completely abolished when either the WIRS motif or the WIRS-binding site in the WRC is mutated. This suggests that DCC may have a second sequence that can interact with the WRC. Our rescue assays in the *Drosophila* ventral nerve cord indicate that $DCC^{\Delta WIRS}$ maintains greater signaling activity than the analogous $Fra^{\Delta WIRS}$ mutation (fig. S7), consistent with the idea that DCC may engage the WRC through two distinct binding sites. Several other neuronal proteins, including HPO-30, retrolinkin, and cannabinoid receptor CB1, were found to interact with the WRC without using a WIRS motif (*54*–*57*). However, DCC shares little sequence similarity with these proteins, suggesting that the second binding sequence on DCC may be distinct. Whether this additional binding site in DCC reflects redundancy in WRC binding or serves to locally enrich WRC to cooperatively activate Arp2/3 remains to be investigated (*58*, *59*). Although we cannot exclude the possibility that mutating the WIRS motif might have WRC-independent effects, our biochemical, functional, and genetic experiments strongly converge on an essential role for the WRC downstream of DCC.

Given the importance of the WIRS motif in DCC/Fra signaling in axon guidance, it may also be important in other DCC/Fra-dependent processes. DCC and Fra have numerous functions in

development and disease outside of the nervous system. DCC was originally identified as a tumor suppressor gene and can promote cell death. DCC can act as a dependence receptor to promote apoptosis in the absence of netrin-1 in several tissues, including colon carcinoma cells and neuroblastomas (*60*–*62*). Fra plays a role in the formation of midgut epithelium in *Drosophila* as well as in heart and lung morphogenesis (*48*, *63*). More recently, our laboratory identified a role for Fra in the *Drosophila* ovary where it promotes germline survival through the inhibition of apoptosis (*64*). Fra also acts in epithelial cells to maintain adherens junctions (AJs) and can regulate the localization of AJ proteins (*65*, *66*). This is especially interesting given that neogenin was recently found to regulate AJ integrity and stability through its interaction with the WRC through its canonical WIRS motif (*67*). This might suggest a shared downstream mechanism by which axon guidance receptors regulate AJs through their WIRS-WRC interactions. Given their extensive involvement in development and disease contexts, a complete dissection of the DCC/Fra signaling pathway is an important area for future investigation.

MATERIALS AND METHODS

Drosophila stocks

The following *Drosophila* strains were used: w^{1118}, fra^{3}, $scar^{\Delta 37}$, *eg-Gal4*, *UAS-CD8GFP II*, *UAS-tau-myc-gfp II*, *ap-Gal4*, *elav-Gal4*, fra^{4}, fra^{6}, *UAS-FraΔC*, *10xUAS-Fra-Myc 86Fb*, *10xUAS-FraΔP2-Myc 86Fb*, *5xUAS-Fra-Myc 86Fb*, and *10xUAS-HSPC300-GFP 86Fb*. Fly strains $hspc300^{\Delta 54.3}$ and $cyfip^{\Delta 85.1}$ were a gift from A. Giangrande (French National Center for Scientific Research). The following transgenic stocks were generated: *10xUAS-FraΔWIRS-Myc 86Fb*, *5xUAS-FraΔWIRS-Myc 86Fb*, *10xUAS-Myc-Dcc 86Fb*, *10xUAS-Myc-DccΔWIRS 86Fb*, and *10xUAS-Myc-DccR1343H 86Fb.* Transgenic flies were generated by BestGene Inc. (Chino Hills, CA) using ΦC31-directed site-specific integration into landing sites at cytological position 86Fb. All crosses were carried out at 25°C.

Mice and rats

Timed pregnant female CD-1 mice were obtained from Charles River Laboratories. Animal work was approved by the Institutional Animal Care and Use Committee of the University of Pennsylvania. Staged pregnant Sprague-Dawley rats were obtained from Charles River Laboratories (New York, USA). Animal work was performed in accordance with the Canadian Council on Animal Care Guidelines and approved by the IRCM Animal Care Committee. Embryos of both sexes (not determined) were randomly used for spinal cord explants and primary dissociated neuron cultures.

Dissociated commissural neuron culture

Primary mouse commissural neuron cultures were prepared as described previously (*35*) and maintained at 5% CO_2 in a humidified incubator. Briefly, commissural neurons were isolated from E12 mouse dorsal spinal cords and plated on acid-washed coverslips coated with poly-D-lysine (Sigma-Aldrich, #P6407) and N-cadherin (2 μg/ml; R&D, #1388-NC). The neurons were cultured in Neurobasal medium supplemented with 10% heat-inactivated fetal bovine serum (FBS) (Gibco, #10437-028) and 1× penicillin-streptomycin/glutamine (Gibco, #10378-016). Dissociated rat commissural neuron cultures were prepared as described previously (*34*, *68*). Briefly, tissue culture plates or acid-washed and sterilized glass coverslips were coated with poly-L-lysine (PLL, Sigma-Aldrich, # P4707, 100 μg/ml for 1.75 to 2 hours). The dorsal one-fifth of the spinal cord of E13 rat neural tubes were microdissected and quickly washed once in cold Ca^{2+}-/Mg^{2+}-free Hanks' balanced salt solution (HBSS). The tissue fragments were trypsinized with 0.15% trypsin in Ca^{2+}-/Mg^{2+}-free HBSS for 7 min at 37°C. Deoxyribonuclease (Worthington, LS002139) and $MgSO_4$ were added briefly for a final concentration of 150 U/ml and 0.15%, respectively. The tissue fragments were then washed in warm Ca^{2+}-/Mg^{2+}-free HBSS and triturated in Ca^{2+}-/Mg^{2+}-free HBSS to yield a suspension of single cells. Cells were plated in Neurobasal medium supplemented with 10% heat-inactivated FBS and 2 mM GlutaMAX (Life Technologies, 35050-061). After ~21 hours, the medium was changed to Neurobasal supplemented with 2% B27 (Life Technologies, 17504-044) and 2 mM GlutaMAX. Commissural neurons were used for experiments after 2 days of culture in vitro. For Dunn chamber experiments, electroporated commissural neurons were plated at 260,000 to 300,000 cells per well in six-well plates on acid-washed PLL-coated 18-mm square #3D coverslips (Assistent, Germany). For immunostaining, commissural neurons were plated at 35,000 cells per well in 24-well plates on acid-washed PLL-coated 12-mm round #1D coverslips. For biochemical experiments, commissural neurons were plated at 0.8 to 1×10^{6} cells per well in PLL-coated six-well plates.

Explant culture

Dorsal spinal cord explants from E12 mouse embryos were dissected and cultured in collagen gels as described previously (*35*). Briefly, the explants were cultured in 50% OptiMEM (Gibco, #31985-070) and 45% Ham's F-12 (Gibco, #11765-054) medium supplemented with 5% horse serum (HS) (Gibco, #16050122), 0.75% glucose (Thermo Fisher Scientific, #D16-500) and 1× penicillin-streptomycin/glutamine for 24 hours.

Cell culture

Drosophila $S2R^{+}$ cells (DGRC, catalog no. 150) were maintained at 25°C in Schneider's media (Life Technologies, #21720024) supplemented with 10% (v/v) FBS and 1% penicillin-streptomycin. The cell line was validated using morphology and doubling time. The cells grew as a loose semi-adherent monolayer with a doubling time of about 40 hours. HEK 293T cells [American Type Culture Collection (ATCC), CRL-3216] were maintained at 37°C and 5% CO_2 in a humidified incubator in Dulbecco's modified Eagle's medium (DMEM, Gibco, #11965084) supplemented with 10% (v/v) FBS and 1% penicillin-streptomycin. The cells were authenticated by short tandem repeat (STR) profiling using ATCC cell line authentication services. Mycoplasma testing was negative for both cell lines. COS7 cells were maintained in DMEM supplemented with 10% FBS and penicillin-streptomycin (Invitrogen) in a 37°C and 5% CO_2 humidified incubator. The COS7 cell line has not been authenticated.

Molecular biology

To generate the *p10xUAST-*$Fra^{\Delta WIRS}$*-Myc* and the *p5xUAST-*$Fra^{\Delta WIRS}$*-Myc* constructs, the wild-type Fra coding sequences from *p10xUAST-Fra-Myc* (*69*) and the *p5xUAST-Fra-Myc* constructs were subcloned into the smaller pBlueScript backbone, and point mutations were introduced into the WIRS motif of the Fra coding sequences with the Quikchange II site-directed mutagenesis kit (Agilent, #200523) using the following primers: GGCCATCCTCTAAAGGCCGCTAGTGTGCCGGGGCCA and TGGCCCCGGCACACTAGCGGCC-

TTTAGAGGATGGCC. The mutated Fra coding sequences were then subcloned back into the respective vectors with 10xUAS or 5xUAS sequences and an attB site for ΦC31-directed site-specific integration.

pcDNA3.1-DCC^{WT}-HA was constructed by subcloning the human DCC coding sequence into pcDNA3.1-Rat Dcc^{WT}-3xHA (from M. Tessier-Lavigne, Stanford University). pcDNA3-DCC$^{\Delta cyto}$-HA expresses DCC without the cytoplasmic domain. To generate the *pcDNA3-DCC$^{\Delta WIRS}$-HA* construct, the following primers were used to mutate the WIRS motif in the *pcDNA3-DCC^{WT}-HA* construct using the Quikchange II site-directed mutagenesis kit (Agilent, #200523): CAACTCACCCACTCCGCGCCGCTGCTAATCCTTTGCTACC and GGTAGCAAAGGATTAGCAGCGGCGCGGAGTGGGTGAGTTG. pcDNA3.1-DCC^{R1343H}-HA (c.4028G > A, p.R1343H) was derived from pcDNA3.1-DCC^{WT}-HA using In-Fusion (Clontech, 639648). Next, the *DCC^{WT}-HA*, *DCC$^{\Delta WIRS}$-HA*, and *DCC^{R1343H}-HA* coding sequences were subcloned into a pCAG vector (a gift from A. Kania, Montreal Clinical Research Institute) using the following primers with *Not*I and *Xho*I sites: GCTAGCGGCCGCATGGAGAATAGTCTTAG and GCTGCTCGAGTCAAGCGTAATCTGGAAC. Gibson assembly (NEB, #E5510S) was used to make the Myc-tagged DCC constructs using the following primers for DCC, CATCACCATCACCATCACGGATCTCATCTTCAAGTAACCGGTTTTC and CTAGACTCGAGCGGCCGCCACTTTAAAAGGCTGAGCCTGTGATG, and the following primers for a pcDNA3.1 plasmid with N-terminal Myc and His tags and a C-terminal V5 tag, CATCACAGGCTCAGCCTTTTAAAGTGGCGGCCGCTCGAGTCTAG and GAAAACCGGTTACTTGAAGATGAGATCCGTGATGGTGATGGTGATG. The Myc-DCC variants were then subcloned into the pCAG vector using the following primers with *Not*I and *Xho*I sites: TATATAGCGGCCGCATGGGCTGGCTCAGG and GGCGCTCGAGTTAAAAGGCTGAGCCTGT.

pcDNA3-Human WAVE1-Flag was a gift from J. D. Scott (University of Washington). pSecTagB-Fc was made by removal of Robo1 from the pSecTagB-Robo1-Fc plasmid. pCep4-Netrin$_{V1.V}$-Fc was a gift from L. Hinck (University of California, Santa Cruz) (*28*).

siRNA generation and validation

The siRNA for knockdown of rat *Dcc* was a predesigned siRNA from IDT whose Design ID is rn.Ri.Dcc.13.1. siRNA oligonucleotides were annealed by incubation at 94°C for 2 mins and cooling down at room temperature and were then aliquoted and stored at −20°C. The efficiency and specificity of the siRNA was evaluated in cultured commissural neurons (fig. S4).

The siRNAs used were as follows: scrambled siRNA, 5′-rUrCrArCrArArGrGrGrArGrGrArArArArGrArGrArGrGrArArGrGrA-3′, 5′-rCrUrUrCrCrUrCrUrCrUrUrUrCrUrCrUrCrCrCrUrUrGrUGA-3′, and *Dcc* siRNA: 5′-rGrGrArArUrCrArArArGrCrArArArGrArUrGrGrUrCrArUGA-3′, 5′-rUrCrArUrGrArCrCrArUrCrUrUrUrGrCrUrUrUrGrArUrUrCrCrUrG-3′. "r" denotes ribonucleotides; two deoxyribonucleotides are present at the 3′ end.

Recombinant protein expression and purification

(MBP)$_2$-WRCs were purified as previously described (*22*). Human WRC contained CYFIP1, NCKAP1, WAVE1 (1–178), ABI2 (1–158), and (MBP)$_2$-HSPC300, with the AW mutant containing ABI2 (1–158)$^{R106A/G110W}$ (*22*). *Drosophila* WRC contained Cyfip, Nap, WAVE (1–181), Abi (1–170), and (MBP)$_2$-HSPC300 (*22*). GST-DCC^{cyto}, GST-dFra^{cyto}, and corresponding mutants were expressed in ArcticExpress (DE3) RIL cells (Agilent) after induction with 0.75 mM isopropyl-β-D-thiogalactopyranoside at 10°C for 16 hours and then purified through glutathione sepharose beads (Cytiva) and anion exchange chromatography using a Source 15Q column (Cytiva) at pH 8.0. GST-DCC^{cyto}proteins were further purified by size exclusion chromatography through a Superdex 200 Increase column (Cytiva). Chemically synthesized WIRS peptides derived from human protocadherin-10 were previously described (*22*).

Pull-down assay

MBP pull-down assays were performed as previously described (*22*). Briefly, 15 to 20 μl of amylose beads (New England Biolabs) was mixed with (MBP)$_2$-WRC (bait) and GST-DCC^{cyto}/GST-Fra^{cyto} (prey) in 1 ml of pull-down buffer [10 mM Hepes (pH 7.0), 50 to 150 mM NaCl as indicated in figure legends, 5% (w/v) glycerol, and 5 mM 2-mercaptoethanol]. The samples were mixed at 4°C for 30 min, washed three times with 1 ml of pull-down buffer, and eluted with 40 μl of elution buffer containing 2% (w/v) maltose. The eluted samples were analyzed by Coomassie blue–stained SDS–polyacrylamide gel electrophoresis (SDS-PAGE) gels. ImageJ (Fiji) was used to quantify the pull-down signals (intensity of the GST-DCC^{cyto} bands). The intensity from the buffer control lane was subtracted from each protein, and the corrected intensity was normalized to the intensity of the DCC$^{WT\text{-}cyto}$ lane.

Western blotting

Cells were lysed with SLB (10 mM tris, 150 mM NaCl, and 0.5% NP-40) with protease inhibitors (Roche, #11873580001) and phosphatase inhibitors (Roche, #04906837001) and boiled in SDS sample buffer for 5 min. The protein samples were separated by SDS-PAGE and transferred to polyvinylidene difluoride membrane. The membranes were blocked with 5% skim milk in TBST [0.01 M tris-HCl (pH 7.5), 150 mM NaCl, and 0.1% Tween20], followed by primary antibody incubation in 1% skim milk in TBST. Secondary antibodies were conjugated to HRP, and Western blots were visualized with chemiluminescence.

Coimmunoprecipitation

Immunoprecipitations from *Drosophila* cells were performed as described previously (*35*). Briefly, S2R$^+$ cells were transiently transfected using Effectene transfection reagent (Qiagen, Valencia CA, #301425) and induced 24 hours later with 0.5 mM copper sulfate. Twenty-four hours after induction, the cells were lysed in TBS-V [150 mM NaCl, 10 mM tris (pH-8), and 1 mM ortho-vanadate] supplemented with 0.5% Surfact-AMPS NP-40 (Thermo Fisher Scientific, Waltham MA, #85124) and 1× cOmplete Protease Inhibitor (Roche, #11697498001) for 20 min at 4°C. Soluble proteins were recovered by centrifugation at 15,000*g* for 10 min at 4°C. Lysates were precleared with 30 μl of a 50% slurry of protein A (Invitrogen, #15918-014) and protein G agarose beads (Invitrogen, #15920-010) by incubation for 20 min at 4°C. Precleared lysates were then incubated with 0.7 μg of rabbit anti-GFP antibody for 2 hours at 4°C to precipitate HSPC300-GFP. Thirty microliters of a 50% slurry of protein A and protein G agarose beads was added, and samples were incubated for an additional 30 min at 4°C. The immunocomplexes were washed three times with lysis buffer, boiled for 10 min in 2× Laemmli SDS sample buffer (Bio-Rad, #1610737), and analyzed by Western blotting. The antibodies used were as follows: rabbit anti-GFP (1:500, Invitrogen, #a11122), mouse anti-Myc (1:1000, DSHB,

#9E10-C), mouse anti-HA (1:500, BioLegend, #901502), HRP goat anti-rabbit (1:10,000, Jackson Immunoresearch, #111-035-003), and HRP goat anti-m21ouse (1:10,000, Jackson Immunoresearch, #115-035-146).

For coimmunoprecipitation assays in *Drosophila* embryos, embryonic protein lysates were prepared from approximately 100 μl of embryos overexpressing *UAS-HSPC300-GFP* alone or with Myc-tagged *UAS-Fra* variants in all neurons. The embryos were lysed in 0.5 ml of TBS-V [150 mM NaCl, 10 mM tris (pH 8.0), and 1 mM ortho-vanadate] supplemented with 1% Surfact-AMPS NP-40 and protease inhibitors by manual homogenization using a plastic pestle. Homogenized samples were incubated with gentle rocking at 4°C for 10 min and centrifuged at 15,000*g* for 10 min in a prechilled rotor. Supernatants were collected after centrifugation, and immunoprecipitations and Western blotting were performed as described above. The antibodies used were as follows: rabbit anti-GFP (1:500, Invitrogen, #a11122), mouse anti-Myc (1:1000, DSHB, #9E10-C), mouse anti–β-tubulin (1:1000, DSHB, #E7), HRP goat anti-rabbit (1:10,000, Jackson Immunoresearch, #111-035-003), and HRP goat anti-mouse (1:10,000, Jackson Immunoresearch, #115-035-146).

For coimunoprecipitation assays in HEK293 cells, HEK293 cells were transfected with the indicated expression vectors using Lipofectamine 3000 (Life Technologies L3000-015). Forty-eight hours after transfection, the cells were lysed with SLB lysis buffer (10 mM tris, 150 mM NaCl, and 0.5% NP-40) with protease inhibitors (Roche, #11873580001) and phosphatase inhibitors (Roche, #04906837001). One to two milligrams of protein lysate in 750 μl of SLB buffer with protease and phosphatase inhibitors was incubated with 2.5 to 5 μg of anti-Flag antibody (Sigma-Aldrich, #F3165) or 0.5 to 1.0 μg of anti-DCC antibody (R&D, #AF844) for 2 hours at 4°C. Protein A/G-agarose beads (Santa Cruz Biotechnology, sc-2003) were added and incubated overnight to capture the immunoprecipitated proteins. The beads were washed three times with SLB buffer, and the proteins binding to the beads were eluted by adding SDS sample buffer and heating at 95°C for 5 min. The immunoprecipitated proteins were analyzed by SDS-PAGE and Western blotting using the following antibodies: anti-HA (Sigma-Aldrich, H3663; clone 12CA5, 1:1000), anti-Flag (Sigma-Aldrich, F3165; 1:1000), anti-DCC (R&D, AF844; 1:1000), and anti–β-actin (Sigma-Aldrich, A5411; 1:5000).

Immunostaining

Dechorionated, formaldehyde-fixed *Drosophila* embryos were fluorescently stained using standard methods. The following antibodies were used: rabbit anti-GFP (1:250; Invitrogen, #a11122), chick anti–β-gal (1:500; Abcam, #ab9361), mouse anti-Myc (1:1000; DSHB, #9E10-C), Alexa Fluor 488 goat anti-rabbit (1:500, Invitrogen, #A11034), Alexa Fluor 488 goat anti-chick (1:500, Invitrogen, #A11039), Cy3 goat anti-mouse (1:500, Jackson Immunoresearch, #115-165-003), Cy3 goat anti-chick (1:500, Abcam, #ab97145), and 647 goat anti-HRP (1:1,000, Jackson Immunoresearch, #123-605-021). The embryos were filleted and mounted in 70% glycerol/1× phosphate-buffered saline (PBS). Dissociated mouse commissural neurons were fixed for 20 min in 4% paraformaldehyde (PFA) (Electron Microscopy Services, #15710) at room temperature and washed three times with PBS. Fixed neurons were then permeabilized with 0.1% Triton X-100 in PBS (PBT) for 10 min and blocked with 2% HS in PBT for 30 min at room temperature. The blocking solution was replaced with primary antibody diluted in 2% HS in PBT and incubated overnight at 4°C. After three washes with PBT, secondary antibody diluted in 2% HS in PBT was added and incubated for 1 hour at room temperature. The neurons were then washed three times with PBT, and the coverslips were mounted in Aquamount. The following antibodies were used: mouse anti-Myc (1:500, DSHB, #9E10-C), Cy3 donkey anti-goat (1:500, Jackson Immunoresearch, #705-165-147), and 488 donkey anti-mouse (1:500, Jackson Immunoresearch, #715-545-150).

Collagen-embedded explants were fixed in 4% PFA overnight at 4°C and washed three times for 10 min in PBS. Fixed explants were then blocked in 2.5% normal goat serum in PBT for 2 hours at room temperature and incubated with primary antibody diluted in blocking solution overnight at 4°C. The explants were washed six times for 1 hour with PBT and incubated with secondary antibody diluted in blocking solution overnight at 4°C. After six 1-hour washes with PBT, the explants were mounted on cavity slides. The following antibodies were used: mouse anti-Myc (1:500, DSHB, #9E10-C), mouse anti–β-tubulin (1:300, DSHB, #E7), rabbit anti-dsRed (1:200, Takara, #632496), Alexa Fluor 488 goat anti-mouse (1:500, Invitrogen, #A11029), and Cy3 goat anti-rabbit (1:500, Jackson Immunoresearch, #111-165-003).

Fixed samples of *Drosophila* embryo nerve cords and dissociated mouse commissural neurons were imaged using a spinning disk confocal system (PerkinElmer) built on a Nikon Ti-U inverted microscope using a Nikon 40× objective with Volocity imaging software. Mouse dorsal spinal cord explants were imaged on a Zeiss LSM 800 microscope with a 10× objective. The images were processed using NIH ImageJ software.

For immunostaining of dissociated rat commissural neuron cultures, the neurons were fixed with 4% PFA at 37°C for 15 min. Dissociated neurons were blocked for 1 hour with PBT with 10% donkey serum at room temperature. The primary antibody (anti-HA, Cell Signaling Technology, 3724; 1:500) was then incubated at 4°C in PBT with 1% donkey serum overnight. After three washes with PBT with 1% donkey serum, the secondary antibodies were incubated in PBT with 1% donkey serum. The nuclei were stained with 4′,6-diamidino-2-phenylindole (Sigma-Aldrich, D95964), and samples were mounted in Mowiol 4-88 (Sigma-Aldrich, 81381). Images of fluorescence immunostaining of commissural neuron cultures were obtained with a Leica DM6 microscope with a 60× objective.

Conditioned media

COS7 cells were transfected using Lipofectamine 3000 (Thermo Fisher Scientific) with pSecTagB-Fc or pCep4-Netrin$_{VI.V}$-Fc. The cells were cultured in OptiMEM without serum. Conditioned medium was collected 2 days after transfection, and the amount of netrin present in the conditioned media was evaluated by Western blot.

Netrin cell surface–binding assay

The netrin cell-surface–binding assay was adapted from (*28*). COS7 cells were cultured on glass coverslips coated with PLL (100 μg/ml for 2 hours) and transfected using Lipofectamine 3000 (Thermo Fisher Scientific) with pcDNA3.1-DCC^{WT}-HA, pcDNA3.1-DCC^{R1343H}, or pCAGs-DCC$^{\Delta WIRS}$. After 2 days, the cells were incubated with 2 μg/ml of control (pSecTagB-Fc) or Netrin$_{VI.V}$-Fc (pCep4-Netrin$_{VIV}$-Fc) conditioned medium in binding buffer (PBS with Ca^{2+} and Mg^{2+} supplemented with 10% HS, 0.1% sodium azide, and 2 μg/ml heparin) at room temperature for 90 min. After gently washing two times with binding buffer and two times with PBS, the cells were

fixed with methanol at −20°C for 12 min and immunostained using standard protocols. The following antibodies were used: anti-DCC (BD, 554223, 1:500), anti-HA (Cell Signaling Technology, NEB, 3724S, clone C29F4, 1:1000), donkey anti-mouse immunoglobulin G (IgG)–DyLight 647 (Jackson ImmunoResearch, 715-605-151, 1:1000), donkey anti-rabbit IgG-488 (Jackson ImmunoResearch, 711-545-152, 1:1000), and donkey anti-human Fc IgG-Cy3 (Jackson ImmunoResearch, 709-165-149, 1:2000). Images of fluorescence immunostaining were obtained with a Leica DM6 microscope with a 63× objective. For quantification, the Fc fluorescence signal (after subtraction of the background fluorescence signal) was normalized according to DCC or HA expression levels (after subtraction of the background fluorescence signal).

Proximity ligation assay

Dissociated commissural neurons were stimulated with BSA (0.1 μg/ml) or Netrin-1 (R&D Systems, #1109-N1-025) for 5 or 30 min and fixed with 4% PFA in PBS. The samples were then blocked with 5% BSA (IgG free) and 0.1% PBT (pH 7.4) for 1 hour at room temperature and then incubated with antibodies against Dcc (R&D Systems, AF844) and Cyfip2 (Abcam, #79716) and diluted in PBS with 1% BSA (IgG free) and 0.1% Triton X-100, overnight at 4°C. The proximity ligation reaction was performed with the Duolink In situ PLA kit (Sigma-Aldrich) according to the manufacturer's instructions.

Electroporation of mouse embryos

Electroporations and dissections of mouse embryos were performed as described previously (*35*). Briefly, E12 mouse embryos were electroporated ex utero by injecting DNA (500 ng/μl) in electroporation buffer [30 mM Hepes (pH7.5) (Thermo Fisher Scientific, #BP299-1), 300 mM KCl (Thermo Fisher Scientific, #BP366-1), 1 mM $MgCl_2$ (Thermo Fisher Scientific, #BP214-500), and 0.1% Fast Green FCF (Thermo Fisher Scientific, #F99-10)] into the central canal of the neural tube. A BTX ECM 830 electroporator (BTX Harvard Apparatus, #45-0662) was used for bilateral electroporation into spinal cord neurons (five 30-V pulses, each of 50-ms duration for each half of the spinal cord). After electroporation, the dorsal spinal cords were dissected out and cut into explants for the explant outgrowth assay or used for preparation of dissociated neuronal cultures.

Electroporation of dissociated commissural neurons

Dissociated rat commissural neurons were electroporated with the Amaxa 96-well Shuttle using the P3 Primary Cell 96-well Nucleofector Kit (Lonza, Switzerland). For each electroporation in one well (20 μl) of a 96-well Nucleofector plate, 5 to 6 × 10^5 commissural neurons were electroporated with 0.25 μg of plasmid DNA and/or 1 μM siRNA. The electroporation was performed with the program 96-CP-100 according to the manufacturer's instructions.

Explant outgrowth assay

Dorsal spinal cord explants from E12 mouse embryos were dissected and cultured in collagen gels as previously described (*32*). Briefly, the explants were embedded in rat tail collagen (Corning, #354249) gels at a distance of one explant diameter away from a mock 293T cell aggregate (ATCC, CRL-3216) or a cell aggregate expressing netrin (pG-netrin-Myc). Explants were grown in 50% OptiMEM and 45% Ham's F-12 medium supplemented with 5% HS, 0.75% glucose, and 1× penicillin-streptomycin/glutamine for 24 hours. The explants were subsequently fixed and stained as described above.

Dunn chamber assay and analysis

To quantify the axon turning of dissociated commissural neurons in response to gradients, we performed the Dunn chamber axon guidance assay as described previously (*34*). Electroporated commissural neurons were grown on PLL-coated square #3D coverslips as described above. The coverslips were then assembled into Dunn chambers. Gradients were generated in the Dunn chamber with netrin-1 (200 ng/ml; R&D Systems, #1109-N1-025) in the outer well. After Dunn chamber assembly, time-lapse phase contrast images were acquired for 2 hours at 37°C with a 10× or 20× fluotar objective on a Leica DMIRE2 inverted microscope (Leica, Germany) equipped with a MS-2000 XYZ automated stage (ASI, Eugene, OR). Images were acquired with an Orca ER charge-coupled device camera (Hamamatsu) using Volocity (Improvision, Waltham, MA). The angle turned was defined as the angle between the original direction of the axon and a straight line connecting the base of the growth cone from the first to the last time point of the assay period.

Quantification and statistical analysis

For analysis of *Drosophila* nerve cord phenotypes, image analysis was conducted blind to the genotype. Data are presented as mean values ± SEM. For statistical analysis, comparisons were made between two groups using the Student's *t* test. For multiple comparisons, significance was assessed using one-way analysis of variance (ANOVA) with Tukey's post hoc tests. Differences were considered significant when $P < 0.05$. To measure Myc signal intensity for DCC quantification in dissociated neurons, Myc-positive neurons were carefully traced in ImageJ and integrated signal density in the traced region was obtained. Background signals were subtracted and mean fluorescence intensity calculated as an integrated signal density per area that is presented in graphs. Data are presented as mean values ± SEM. For statistical analysis, comparisons were made using one-way ANOVA with Tukey's post hoc tests. Differences were considered significant when $P < 0.05$. For the explant outgrowth assay, explant images were converted to black-and-white composites using the autothreshold (Li) function. Explant quadrants were delineated by placing a right-angled crosshair at the center of each explant with the proximal quadrant directly facing the cell aggregate. The total area of black pixels was measured for the proximal and distal quadrants using the Analyze Particles function. The particles showing axonal outgrowth were then erased using the Eraser tool, and the total area of black particles was measured again. The difference was recorded as total area of axonal outgrowth. Next, the length of each quadrant was measured by tracing the border of the quadrant using the Freehand Line tool. Values for the total area of outgrowth were normalized to the length of the quadrant, and these final values were used to obtain the proximal/distal ratios for each explant. The measurements for each explant in a set were averaged, and the ratios of experimental conditions compared with control condition were calculated. Data are presented as means ± SEM. For statistical analysis, comparisons were made between groups using one-way ANOVA with Tukey's post hoc tests. Differences were considered significant when $P < 0.05$. For Western blots, densitometric analysis was performed and band intensities of coimmunoprecipitating proteins in the immunoprecipitates were normalized to band intensities of HSPC300 in the immunoprecipitates as well as to lysate levels of

the coimmunoprecipitating proteins. For each independent experiment, the values were normalized to wild-type Fra. Data are presented as means ± SEM. For statistical analysis, significance was assessed using one-way ANOVA with Tukey's post hoc tests. Differences were considered significant when $P < 0.05$. For all graphs, $*P < 0.05$, $**P < 0.01$, $***P < 0.001$, and $****P < 0.0001$. Details on the statistics for fig. S7 are as follows: The average EW axon crossing defect was obtained for the *fra*^{3} control groups of each experiment. Each experimental group data point was then normalized to the computed average of their respective sibling control group, generating normalized percent segments with EW crossing defects. All distributions were then tested for normality using the Shapiro-Wilk test. All failed normality testing; therefore, nonparametric tests were used. All statistics and graphs were generated using GraphPad Prism 9.

Supplementary Materials

The PDF file includes:
Figs. S1 to S8

Other Supplementary Material for this manuscript includes the following:
MDAR Reproducibility Checklist

REFERENCES AND NOTES

1. M. Gorla, G. J. Bashaw, Molecular mechanisms regulating axon responsiveness at the midline. *Dev. Biol.* **466**, 12–21 (2020).
2. S. W. Moore, M. Tessier-Lavigne, T. E. Kennedy, Netrins and their receptors. *Adv. Exp. Med. Biol.* **621**, 17–31 (2007).
3. L. Izzi, F. Charron, Midline axon guidance and human genetic disorders. *Clin. Genet.* **80**, 226–234 (2011).
4. S. S. Jamuar, K. Schmitz-Abe, A. M. D'Gama, M. Drottar, W.-M. Chan, M. Peeva, S. Servattalab, A.-T. N. Lam, M. R. Delgado, N. J. Clegg, Z. A. Zayed, M. A. Dogar, I. A. Alorainy, A. A. Jamea, K. Abu-Amero, M. Griebel, W. Ward, E. S. Lein, K. Markianos, A. J. Barkovich, C. D. Robson, P. E. Grant, T. M. Bosley, E. C. Engle, C. A. Walsh, T. W. Yu, Biallelic mutations in human DCC cause developmental split-brain syndrome. *Nat. Genet.* **49**, 606–612 (2017).
5. A. P. L. Marsh, D. Heron, T. J. Edwards, A. Quartier, C. Galea, C. Nava, A. Rastetter, M.-L. Moutard, V. Anderson, P. Bitoun, J. Bunt, A. Faudet, C. Garel, G. Gillies, I. Gobius, J. Guegan, S. Heide, B. Keren, F. Lesne, V. Lukic, S. A. Mandelstam, G. M. Gillivray, A. M. Ilroy, A. Méneret, C. Mignot, L. R. Morcom, S. Odent, A. Paolino, K. Pope, F. Riant, G. A. Robinson, M. Spencer-Smith, M. Srour, S. E. M. Stephenson, R. Tankard, O. Trouillard, Q. Welniarz, A. Wood, A. Brice, G. Rouleau, T. Attié-Bitach, M. B. Delatycki, J.-L. Mandel, D. J. Amor, E. Roze, A. Piton, M. Bahlo, T. B. de Villemeur, E. H. Sherr, R. J. Leventer, L. J. Richards, P. J. Lockhart, C. Depienne, Mutations in *DCC* cause isolated agenesis of the corpus callosum with incomplete penetrance. *Nat. Genet.* **49**, 511–514 (2017).
6. M. Srour, J. B. Rivière, J. M. T. Pham, M. P. Dubé, S. Girard, S. Morin, P. A. Dion, G. Asselin, D. Rochefort, P. Hince, S. Diab, N. Sharafaddinzadeh, S. Chouinard, H. Théoret, F. Charron, G. A. Rouleau, Mutations in *DCC* cause congenital mirror movements. *Science* **328**, 592 (2010).
7. Q. Welniarz, M. P. Morel, O. Pourchet, C. Gallea, J. C. Lamy, M. Cincotta, M. Doulazmi, M. Belle, A. Méneret, O. Trouillard, M. Ruiz, V. Brochard, S. Meunier, A. Trembleau, M. Vidailhet, A. Chédotal, I. Dusart, E. Roze, Non cell-autonomous role of DCC in the guidance of the corticospinal tract at the midline. *Sci. Rep.* **7**, 410 (2017).
8. N. P. Boyer, L. E. McCormick, S. Menon, F. L. Urbina, S. L. Gupton, A pair of E3 ubiquitin ligases compete to regulate filopodial dynamics and axon guidance. *J. Cell Biol.* **219**, e201902088 (2020).
9. A. Briançon-Marjollet, A. Ghogha, H. Nawabi, I. Triki, C. Auziol, S. Fromont, C. Piché, H. Enslen, K. Chebli, J.-F. Cloutier, V. Castellani, A. Debant, Trio mediates netrin-1-induced Rac1 activation in axon outgrowth and guidance. *Mol. Cell. Biol.* **28**, 2314–2323 (2008).
10. C. Lebrand, E. W. Dent, G. A. Strasser, L. M. Lanier, M. Krause, T. M. Svitkina, G. G. Borisy, F. B. Gertler, Critical role of Ena/VASP proteins for filopodia formation in neurons and in function downstream of netrin-1. *Neuron* **42**, 37–49 (2004).
11. G. Liu, H. Beggs, C. Jürgensen, H.-T. Park, H. Tang, J. Gorski, K. R. Jones, L. F. Reichardt, J. Wu, Y. Rao, Netrin requires focal adhesion kinase and Src family kinases for axon outgrowth and attraction. *Nat. Neurosci.* **7**, 1222–1232 (2004).
12. S. Menon, N. P. Boyer, C. C. Winkle, L. M. McClain, C. C. Hanlin, D. Pandey, S. Rothenfußer, A. M. Taylor, S. L. Gupton, The E3 ubiquitin ligase TRIM9 is a filopodia off switch required for netrin-dependent axon guidance. *Dev. Cell* **35**, 698–712 (2015).
13. M. Meriane, J. Tcherkezian, C. A. Webber, E. I. Danek, I. Triki, S. McFarlane, E. Bloch-Gallego, N. Lamarche-Vane, Phosphorylation of DCC by Fyn mediates Netrin-1 signaling in growth cone guidance. *J. Cell Biol.* **167**, 687–698 (2004).
14. M. Shekarabi, T. E. Kennedy, The netrin-1 receptor DCC promotes filopodia formation and cell spreading by activating Cdc42 and Rac1. *Mol. Cell. Neurosci.* **19**, 1–17 (2002).
15. C. Chang, C. E. Adler, M. Krause, S. G. Clark, F. B. Gertler, M. Tessier-Lavigne, C. I. Bargmann, MIG-10/lamellipodin and AGE-1/PI3K promote axon guidance and outgrowth in response to slit and netrin. *Curr. Biol.* **16**, 854–862 (2006).
16. R. S. Demarco, E. C. Struckhoff, E. A. Lundquist, The Rac GTP exchange factor TIAM-1 acts with CDC-42 and the guidance receptor UNC-40/DCC in neuronal protrusion and axon guidance. *PLOS Genet.* **8**, e1002665 (2012).
17. D. J. Forsthoefel, E. C. Liebl, P. A. Kolodziej, M. A. Seeger, The Abelson tyrosine kinase, the Trio GEF and enabled interact with the Netrin receptor frazzled in *Drosophila*. *Development* **132**, 1983–1994 (2005).
18. Z. Gitai, T. W. Yu, E. A. Lundquist, M. Tessier-Lavigne, C. I. Bargmann, The netrin receptor UNC-40/DCC stimulates axon attraction and outgrowth through enabled and, in parallel, Rac and UNC-115/AbLIM. *Neuron* **37**, 53–65 (2003).
19. M. P. O'Donnell, G. J. Bashaw, Distinct functional domains of the Abelson tyrosine kinase control axon guidance responses to Netrin and slit to regulate the assembly of neural circuits. *Development* **140**, 2724–2733 (2013).
20. S. Schlienger, P. T. Yam, N. Balekoglu, H. Ducuing, J.-F. Michaud, S. Makihara, D. K. Kramer, B. Chen, A. Fasano, A. Berardelli, F. F. Hamdan, G. A. Rouleau, M. Srour, F. Charron, Genetics of mirror movements identifies a multifunctional complex required for Netrin-1 guidance and lateralization of motor control. *Sci. Adv.* **9**, eadd5501 (2023).
21. M. L. C. Hutchinson, J. St-Onge, S. Schlienger, N. Boudrahem-Addour, L. Mougharbel, J.-F. Michaud, C. Lloyd, E. Bruneau, C. Roux, A. N. Sahly, B. Osterman, K. A. Myers, G. A. Rouleau, D. A. Jimenez Cruz, J.-B. Rivière, A. Accogli, F. Charron, M. Srour, Defining the genetic landscape of congenital mirror movements in 80 affected individuals. *Mov. Disord.* **39**, 400–410 (2024).
22. B. Chen, K. Brinkmann, Z. Chen, C. W. Pak, Y. Liao, S. Shi, L. Henry, N. V. Grishin, S. Bogdan, M. K. Rosen, The WAVE regulatory complex links diverse receptors to the actin cytoskeleton. *Cell* **156**, 195–207 (2014).
23. K. G. Campellone, M. D. Welch, A nucleator arms race: Cellular control of actin assembly. *Nat. Rev. Mol. Cell Biol.* **11**, 237–251 (2010).
24. D. A. Kramer, H. K. Piper, B. Chen, WASP family proteins: Molecular mechanisms and implications in human disease. *Eur. J. Cell Biol.* **101**, 151244 (2022).
25. K. Rottner, T. E. B. Stradal, B. Chen, WAVE regulatory complex. *Curr. Biol.* **31**, R512–R517 (2021).
26. J. D. Rotty, C. Wu, J. E. Bear, New insights into the regulation and cellular functions of the ARP2/3 complex. *Nat. Rev. Mol. Cell Biol.* **14**, 7–12 (2013).
27. M. L. C. Hutchinson, J. St-Onge, S. Schlienger, N. Boudrahem-Addour, L. Mougharbel, J.-F. Michaud, C. Lloyd, E. Bruneau, C. Roux, A. N. Sahly, B. Osterman, K. A. Myers, G. A. Rouleau, D. A. Jimenez Cruz, J.-B. Rivière, A. Accogli, F. Charron, M. Srour, Defining the genetic landscape of congenital mirror movements in 80 individuals. *Mov. Dis.* **39**, 400–410 (2023).
28. K. Keino-Masu, M. Masu, L. Hinck, E. D. Leonardo, S. S. Y. Chan, J. G. Culotti, M. Tessier-Lavigne, Deleted in colorectal cancer (DCC) encodes a netrin receptor. *Cell* **87**, 175–185 (1996).
29. A. Fazeli, S. L. Dickinson, M. L. Hermiston, R. V. Tighe, R. G. Steen, C. G. Small, E. T. Stoeckli, K. Keino-Masu, M. Masu, H. Rayburn, J. Simons, R. T. Bronson, J. I. Gordon, M. Tessier-Lavigne, R. A. Weinberg, Phenotype of mice lacking functional *deleted in colorectal cancer* (Dcc) gene. *Nature* **386**, 796–804 (1997).
30. T. E. Kennedy, T. Serafini, J. R. de la Torre, M. Tessier-Lavigne, Netrins are diffusible chemotropic factors for commissural axons in the embryonic spinal cord. *Cell* **78**, 425–435 (1994).
31. T. Serafini, S. A. Colamarino, E. D. Leonardo, H. Wang, R. Beddington, W. C. Skarnes, M. Tessier-Lavigne, Netrin-1 is required for commissural axon guidance in the developing vertebrate nervous system. *Cell* **87**, 1001–1014 (1996).
32. T. Serafini, T. E. Kennedy, M. J. Gaiko, C. Mirzayan, T. M. Jessell, M. Tessier-Lavigne, The netrins define a family of axon outgrowth-promoting proteins homologous to *C. elegans* UNC-6. *Cell* **78**, 409–424 (1994).
33. J. M. Cioni, H. H. W. Wong, D. Bressan, L. Kodama, W. A. Harris, C. E. Holt, Axon-axon interactions regulate topographic optic tract sorting via CYFIP2-dependent WAVE complex function. *Neuron* **97**, 1078–1093.e6 (2018).
34. P. T. Yam, S. D. Langlois, S. Morin, F. Charron, Sonic hedgehog guides axons through a noncanonical, Src-family-kinase-dependent signaling pathway. *Neuron* **62**, 349–362 (2009).
35. K. Chaudhari, M. Gorla, C. Chang, A. Kania, G. J. Bashaw, Robo recruitment of the Wave regulatory complex plays an essential and conserved role in midline repulsion. *eLife* **10**, e64474 (2021).

36. A. Schenck, A. Qurashi, P. Carrera, B. Bardoni, C. Diebold, E. Schejter, J. L. Mandel, A. Giangrande, WAVE/SCAR, a multifunctional complex coordinating different aspects of neuronal connectivity. *Dev. Biol.* **274**, 260–270 (2004).
37. D. S. Garbe, M. O'Donnell, G. J. Bashaw, Cytoplasmic domain requirements for frazzled-mediated attractive axon turning at the *Drosophila* midline. *Development* **134**, 4325–4334 (2007).
38. J. A. Zallen, Y. Cohen, A. M. Hudson, L. Cooley, E. Wieschaus, E. D. Schejter, SCAR is a primary regulator of Arp2/3-dependent morphological events in *Drosophila*. *J. Cell Biol.* **156**, 689–701 (2002).
39. P. A. Kolodziej, L. C. Timpe, K. J. Mitchell, S. R. Fried, C. S. Goodman, L. Y. Jan, Y. N. Jan, frazzled encodes a *Drosophila* member of the DCC immunoglobulin subfamily and is required for CNS and motor axon guidance. *Cell* **87**, 197–204 (1996).
40. L. Yang, D. S. Garbe, G. J. Bashaw, A frazzled/DCC-dependent transcriptional switch regulates midline axon guidance. *Science* **324**, 944–947 (2009).
41. C. Santiago, G. J. Bashaw, Islet coordinately regulates motor axon guidance and dendrite targeting through the frazzled/DCC receptor. *Cell Rep.* **18**, 1646–1659 (2017).
42. M. P. O'Donnell, G. J. Bashaw, Src inhibits midline axon crossing independent of frazzled/deleted in colorectal carcinoma (DCC) receptor tyrosine phosphorylation. *J. Neurosci.* **33**, 305–314 (2013).
43. B. Chen, H. T. Chou, C. A. Brautigam, W. Xing, S. Yang, L. Henry, L. K. Doolittle, T. Walz, M. K. Rosen, Rac1 GTPase activates the WAVE regulatory complex through two distinct binding sites. *eLife* **6**, e29795 (2017).
44. B. Ding, S. Yang, M. Schaks, Y. Liu, A. J. Brown, K. Rottner, S. Chowdhury, B. Chen, Structures reveal a key mechanism of WAVE regulatory complex activation by Rac1 GTPase. *Nat. Commun.* **13**, 5444 (2022).
45. X. Li, X. Gao, G. Liu, W. Xiong, J. Wu, Y. Rao, Netrin signal transduction and the guanine nucleotide exchange factor DOCK180 in attractive signaling. *Nat. Neurosci.* **11**, 28–35 (2008).
46. X. Li, E. Saint-Cyr-Proulx, K. Aktories, N. Lamarche-Vane, Rac1 and Cdc42 but not RhoA or Rho kinase activities are required for neurite outgrowth induced by the Netrin-1 receptor DCC (deleted in colorectal cancer) in N1E-115 neuroblastoma cells. *J. Biol. Chem.* **277**, 15207–15214 (2002).
47. F. A. Konopacki, H. H. W. Wong, A. Dwivedy, A. Bellon, M. D. Blower, C. E. Holt, ESCRT-II controls retinal axon growth by regulating DCC receptor levels and local protein synthesis. *Open Biol.* **6**, 150218 (2016).
48. M. Pert, M. Gan, R. Saint, M. J. Murray, Netrins and frazzled/DCC promote the migration and mesenchymal to epithelial transition of *Drosophila* midgut cells. *Biol. Open* **4**, 233–243 (2015).
49. M. Piper, S. Salih, C. Weinl, C. E. Holt, W. A. Harris, Endocytosis-dependent desensitization and protein synthesis-dependent resensitization in retinal growth cone adaptation. *Nat. Neurosci.* **8**, 179–186 (2005).
50. S. Stern, B. J. Hilton, E. R. Burnside, S. Dupraz, E. E. Handley, J. M. Gonyer, C. Brakebusch, F. Bradke, RhoA drives actin compaction to restrict axon regeneration and astrocyte reactivity after CNS injury. *Neuron* **109**, 3436–3455.e9 (2021).
51. R. K. Chance, G. J. Bashaw, Slit-dependent endocytic trafficking of the robo receptor is required for son of sevenless recruitment and midline axon repulsion. *PLOS Genet.* **11**, e1005402 (2015).
52. A. Pignata, H. Ducuing, L. Boubakar, T. Gardette, K. Kindbeiter, M. Bozon, S. Tauszig-Delamasure, J. Falk, O. Thoumine, V. Castellani, A spatiotemporal sequence of sensitization to slits and semaphorins orchestrates commissural axon navigation. *Cell Rep.* **29**, 347–362.e5 (2019).
53. R. E. McConnell, J. Edward van Veen, M. Vidaki, A. V. Kwiatkowski, A. S. Meyer, F. B. Gertler, A requirement for filopodia extension toward slit during Robo-mediated axon repulsion. *J. Cell Biol.* **213**, 261–274 (2016).
54. D. A. Kramer, H. Y. Narvaez-Ortiz, R. Shi, K. Shen, J. Roche, B. J. Nolen, B. Chen, Dendrite branching receptor HPO-30 uses two novel mechanisms to regulate actin cytoskeletal remodeling. bioRxiv 491788 [Preprint] (2022). https://doi.org/10.1101/2022.05.13.491788.
55. C. Njoo, N. Agarwal, B. Lutz, R. Kuner, The cannabinoid receptor CB1 interacts with the WAVE1 complex and plays a role in actin dynamics and structural plasticity in neurons. *PLOS Biol.* **13**, e1002286 (2015).
56. C. Xu, X. Fu, S. Zhu, J. J. Liu, Retrolinkin recruits the WAVE1 protein complex to facilitate BDNF-induced TrkB endocytosis and dendrite outgrowth. *Mol. Biol. Cell* **27**, 3342–3356 (2016).
57. W. Zou, X. Dong, T. R. Broederdorf, A. Shen, D. A. Kramer, R. Shi, X. Liang, D. M. Miller III, Y. K. Xiang, R. Yasuda, B. Chen, K. Shen, A dendritic guidance receptor complex brings together distinct actin regulators to drive efficient F-actin assembly and branching. *Dev. Cell* **45**, 362–375.e3 (2018).
58. S. B. Padrick, H. C. Cheng, A. M. Ismail, S. C. Panchal, L. K. Doolittle, S. Kim, B. M. Skehan, J. Umetani, C. A. Brautigam, J. M. Leong, M. K. Rosen, Hierarchical regulation of WASP/WAVE proteins. *Mol. Cell* **32**, 426–438 (2008).
59. S. B. Padrick, M. K. Rosen, Physical mechanisms of signal integration by WASP family proteins. *Annu. Rev. Biochem.* **79**, 707–735 (2010).
60. Y. Q. Chen, J. T. Hsieh, F. Yao, B. Fang, R. C. Pong, S. C. Cipriano, F. Krepulat, Induction of apoptosis and G2/M cell cycle arrest by DCC. *Oncogene* **18**, 2747–2754 (1999).
61. C. Forcet, X. Ye, L. Granger, V. Corset, H. Shin, D. E. Bredesen, P. Mehlen, The dependence receptor DCC (deleted in colorectal cancer) defines an alternative mechanism for caspase activation. *Proc. Natl. Acad. Sci. U.S.A.* **98**, 3416–3421 (2001).
62. P. Mehlen, S. Rabizadeh, S. J. Snipas, N. Assa-Munt, G. S. Salvesen, D. E. Bredesen, The DCC gene product induces apoptosis by a mechanism requiring receptor proteolysis. *Nature* **395**, 801–804 (1998).
63. F. D. Macabenta, A. G. Jensen, Y. S. Cheng, J. J. Kramer, S. G. Kramer, Frazzled/DCC facilitates cardiac cell outgrowth and attachment during *Drosophila* dorsal vessel formation. *Dev. Biol.* **380**, 233–242 (2013).
64. S. A. Russell, K. M. Laws, G. J. Bashaw, Frazzled/Dcc acts independently of Netrin to promote germline survival during *Drosophila* oogenesis. *Development* **148**, dev199762 (2021).
65. S. Golenkina, V. Chaturvedi, R. Saint, M. J. Murray, Frazzled can act through distinct molecular pathways in epithelial cells to regulate motility, apical constriction, and localisation of E-Cadherin. *PLOS ONE* **13**, e0194003 (2018).
66. R. Manhire-Heath, S. Golenkina, R. Saint, M. J. Murray, Netrin-dependent downregulation of frazzled/DCC is required for the dissociation of the peripodial epithelium in *Drosophila*. *Nat. Commun.* **4**, 2790 (2013).
67. N. K. Lee, K. W. Fok, A. White, N. H. Wilson, C. J. O'Leary, H. L. Cox, M. Michael, A. S. Yap, H. M. Cooper, Neogenin recruitment of the WAVE regulatory complex maintains adherens junction stability and tension. *Nat. Commun.* **7**, 11082 (2016).
68. S. D. Langlois, S. Morin, P. T. Yam, F. Charron, Dissection and culture of commissural neurons from embryonic spinal cord. *J. Vis. Exp.* **39**, 1773 (2010).
69. A. Neuhaus-Follini, G. J. Bashaw, The intracellular domain of the frazzled/DCC receptor is a transcription factor required for commissural axon guidance. *Neuron* **87**, 751–763 (2015).

Acknowledgments: We would like to thank the members of the Bashaw, Charron, Srour, and Chen laboratories for discussions and comments on the manuscript. We thank C. Barrios-Camacho for consultation on statistical analysis. We thank Z. DeLoughery and A. Jaworski for guidance on the in vitro explant experiments. We thank H. Song and G. L. Ming for allowing us to use their laboratory facilities. We thank A. Giangrande, A. Kania, M. Tessier-Lavigne, J. D. Scott, and L. Hinck for sending fly lines or plasmids, as well as BDSC and FlyBase. We thank R. Sauvé for expert technical assistance. **Funding:** This study was supported by the National Institutes of Health (grant R35 GM128786 to B.C.), the Canadian Institutes of Health Research (grants PJT173307, PJT180647, and FDN334023 to F.C.), the Canada Foundation for Innovation (grants CFI33768 and CFI39794 to F.C.), the Canada Research Chair (CRC230496 to F.C.), the National Science Foundation (grants IOS-1853719 and R35 NS097340 to G.J.B.), and the China Scholarship Council (to K.Z.). M.S. receives salary support as a Chercheur-boursier clinicien from the Fonds de recherche du Québec - Santé. F.C. receives salary support as the Canada Research Chair in Developmental Neurobiology. **Author contributions:** Conceptualization: K.C., K.Z., P.T.Y., M.S., B.C., F.C., and G.J.B. Investigation: K.C., K.Z., P.T.Y., Y.Z., D.A.K., S.G., S.S., S.C., J.-F.M., M.C., and J.W. Supervision: P.T.Y., M.S., B.C., F.C., and G.J.B. Writing: K.C., P.T.Y., F.C., and G.J.B. **Competing interests:** The authors declare that they have no competing interests. **Data and materials availability:** All data needed to evaluate the conclusions in the paper are present in the paper or the Supplementary Materials. Reasonable requests for resources and additional information should be directed to and will be fulfilled by the corresponding authors.

Submitted 9 August 2023
Resubmitted 6 May 2024
Accepted 6 September 2024
Published 1 October 2024
10.1126/scisignal.adk2345